Neutron electric dipole moment using N_f=2+1+1 twisted mass fermions

C. Alexandrou[(a,b)], **A. Athenodorou**[(a,b)], **M. Constantinou**[(a,b)], **K. Hadjiyiannakou**[(a,b)], **K. Jansen**[(d)], **G. Koutsou**[(b)] **K. Ottnad**[(a,e)] **M. Petschlies**[(b,e)]

[(a)] Department of Physics, University of Cyprus, P.O. Box 20537, 1678 Nicosia, Cyprus
[(b)] Computation-based Science and Technology Research Center, The Cyprus Institute, 20 Kavafi Str., Nicosia 2121, Cyprus
[(d)] NIC, DESY, Platanenallee 6, D-15738 Zeuthen, Germany
[(e)] Helmholtz-Institut für Strahlen- und Kernphysik (Theorie) and Bethe Center for Theoretical Physics, Universität Bonn, 53115 Bonn, Germany

Abstract

We evaluate the neutron electric dipole moment $|\vec{d}_N|$ using lattice QCD techniques. The gauge configurations analyzed are produced by the European Twisted Mass Collaboration using N_f=2+1+1 twisted mass fermions at one value of the lattice spacing of $a \simeq 0.082$ fm and a light quark mass corresponding to $m_\pi \simeq 373$ MeV. Our approach to extract the neutron electric dipole moment is based on the calculation of the CP-odd electromagnetic form factor $F_3(Q^2)$ for small values of the vacuum angle θ in the limit of zero Euclidean momentum transfer Q^2. The limit $Q^2 \to 0$ is realized either by adopting a parameterization of the momentum dependence of $F_3(Q^2)$ and performing a fit, or by employing new position space methods, which involve the elimination of the kinematical momentum factor in front of $F_3(Q^2)$. The computation in the presence of a CP-violating term requires the evaluation of the topological charge $\mathcal{Q}$. This is computed by applying the cooling technique and the gradient flow with three different actions, namely the Wilson, the Symanzik tree-level improved and the Iwasaki action. We demonstrate that cooling and gradient flow give equivalent results for the neutron electric dipole moment. Our analysis yields a value of $|\vec{d}_N| = 0.045(6)(1)\ \bar{\theta}\ e \cdot \text{fm}$ for the ensemble with $m_\pi = 373$ MeV considered.

March 16, 2016

Contents

1 Introduction

The discrete symmetries of parity P, charge conjugation C and time-reversal T play an important role in the allowed phenomenology described by the Standard Model (SM) of particle physics. An experimental observation of a non-vanishing electric-dipole moment on the neutron would directly signal violation of both P and T symmetries. Violations of P and T can occur in both strong and electroweak sectors of the Standard Model.

So far, a non-vanishing neutron electric dipole moment (nEDM) has not been reported and current bounds are still several orders of magnitude above what one expects from CP violation induced by weak interactions [1], making, thus, nEDM investigations an interesting probe for Beyond the Standard Model (BSM) physics [2]. Several experiments are under way to improve the upper bound on the nEDM, $\vec{d}_N$, with the best experimental upper limit being [3, 4, 5]

$$|\vec{d}_N| < 2.9 \times 10^{-13} e \cdot \text{fm} \ (90\% \ \text{CL}) \, . \tag{1}$$

This result has been extracted at the Institut Laue-Langevin (ILL) reactor in Grenoble by storing "ultra-cold" neutrons and measuring the change in the neutron spin precession frequency in a weak magnetic field when a strong, parallel background electric field is reversing its own sign.

To examine theoretically how an nEDM may arise, we start with the CP-conserving QCD Lagrangian density, which in Euclidean space is given by

$$\mathcal{L}_{\text{QCD}}(x) = \frac{1}{2g^2} \text{Tr}\left[G_{\mu\nu}(x) \, G_{\mu\nu}(x)\right] + \sum_f \overline{\psi}_f(x) \, (\gamma_\mu D_\mu + m_f) \psi_f(x) \ , \tag{2}$$

where ψ_f denotes a fermion field of flavor f with bare mass m_f and $G_{\mu\nu}$ is the gluon field tensor. Eq. (2) is invariant under P and T transformations and, thus, cannot lead to a non-vanishing nEDM. The QCD Lagrangian can be generalized by including an additional CP-violating interaction (Chern-Simons) term given by

$$\mathcal{L}_{\text{CS}}(x) \equiv -i\theta q(x) \ . \tag{3}$$

The so called θ-parameter controls the strength of the CP-breaking and $q(x)$ is the topological charge density, which in Euclidean space is defined as

$$q(x) = \frac{1}{32\pi^2} \epsilon_{\mu\nu\rho\sigma} \text{Tr}\left[G_{\mu\nu}(x) \, G_{\rho\sigma}(x)\right] \ , \tag{4}$$

where $\epsilon_{\mu\nu\rho\sigma}$ is the totally antisymmetric tensor. Although the CP-violating term in Eq. (3) does not modify the equations of motion since it can be expressed as a total divergence, it has observable consequences. In particular, it leads to a non-zero value for the nEDM. In this work, we consider a quantum field theory described by the C-even Lagrangian density

$$\mathcal{L}(x) = \mathcal{L}_{\text{QCD}}(x) + \mathcal{L}_{\text{CS}}(x) \ , \tag{5}$$

with θ taken as a small continuous parameter enabling us to perturbatively expand in terms of θ and only keep first order contributions.

CP violation in the electroweak sector is observed in K and B meson decays and is accounted for by the phase of the CKM matrix. However, this CP-violating phase alone cannot explain the baryon asymmetry of the universe suggesting that there maybe additional sources of CP violation. If one considers the electroweak sector of the Standard Model, the Lagrangian in Eq. (5) gets a contribution from the quark mass matrix M, arising from Yukawa couplings to the Higgs field

$$\bar{\psi}^R_{f_1}(x) M_{f_1 f_2} \psi^L_{f_2}(x) + \bar{\psi}^L_{f_1}(x) M^\dagger_{f_1 f_2} \psi^R_{f_2}(x) \, , \tag{6}$$

with ψ^L_f and ψ^R_f being the left and right handed quark fields with flavour indices f. If one performs a $U(1)_A$ chiral transformation an additional $\epsilon_{\mu\nu\rho\sigma} \text{Tr}\left[G_{\mu\nu} G_{\rho\sigma}\right]$ contribution is introduced because of the chiral anomaly.

Hence, the parameter θ shifts to $\overline{\theta} = \theta + \arg\det M$ where now $\overline{\theta}$ describes the CP-violating parameter of the extended strong and electroweak symmetry. In addition to the experimental investigations that give an upper bound in the nEDM, several model studies [6, 7, 8, 9, 10, 11, 12, 13, 14, 15], as well as more recent effective field theory calculations [16, 17, 18, 19, 20, 21, 22, 23, 24, 25], have attempted to provide a value for the nEDM. They report values in the range of

$$|\vec{d}_N| \sim \bar{\theta} \cdot \mathcal{O}\left(10^{-2} - 10^{-4}\right) e \cdot \text{fm}\,. \tag{7}$$

Using the experimental upper bound (Eq. (1)) and the above prediction we obtain a bound of the order $\bar{\theta} \lesssim \mathcal{O}\left(10^{-9} - 10^{-11}\right)$. Hence, according to these models, $\bar{\theta}$ is indeed very small and possibly zero with the latter resulting in a vanishing value of the nEDM.

Therefore, either θ and $\arg\det M$ are small or they cancel each other at a level that the experimental upper bound on the nEDM is satisfied. No matter which one of these two cases holds, one needs to be able to explain why nature chooses such a small value for $\overline{\theta}$. This is what is referred to as the "strong CP problem". Attempts to explain the smallness of the nEDM invoke new physics as for instance the Peccei-Quinn mechanism [26, 27], which requires the existence of the axion that to date has not been observed. For the purposes of this work we assume that θ is small and keep only leading order contributions in what follows.

The effective Lagrangian giving rise to the nEDM at leading order in $\bar{\theta}$ can be written as [2, 28]

$$-\bar{\theta}\frac{F_3(Q^2)}{4m_N}\bar{u}_N(p_f)\sigma^{\mu\nu}\gamma_5 u_N(p_i)F^{\mu\nu}\,, \tag{8}$$

in Euclidean space. We denote by $u_N(p)$ the nucleon spinor and by $F_{\mu\nu}$ the electromagnetic field tensor, while $\sigma_{\mu\nu} = [\gamma_\mu, \gamma_\nu]/2$ and $p_f(p_i)$ is the final (initial) momentum. m_N denotes the mass of the neutron, $Q^2 = -q^2$ the four-momentum transfer in Euclidean space ($q = p_f - p_i$) and $F_3(Q^2)$ is the CP-odd form factor. The nEDM, $\vec{d}_N$ is then given by [2, 28]

$$|\vec{d}_N| = \bar{\theta} \lim_{Q^2 \to 0} \frac{|F_3(Q^2)|}{2m_N}\,, \tag{9}$$

to leading order in $\bar{\theta}$. In a theory with CP violation we can, therefore, calculate the electric dipole moment by evaluating the zero momentum transfer limit of the CP-odd form factor. This provides the framework on which our investigation will be based. As will be explained in Section 6, the CP-violating nucleon matrix element, decomposes to $Q_k F_3(Q^2)$ (k=1, 2, 3) and not $F_3(Q^2)$ alone, hindering a direct extraction of $F_3(0)$. We adopt two approaches to determine $F_3(0)$: The first one that is commonly applied in lattice QCD computations of form factors, is to take a suitable parameterization of the Q^2-dependence. We take a dipole form for the Q^2-dependence of $F_3(Q^2)$ and perform a fit to extract its value at $Q^2 = 0$. The second approach is a new method that we have recently developed to compute form factors directly at $Q^2 = 0$, extracted from matrix elements that involve a multiplicative kinematical factor of $\vec{Q}$ [29]. To this end we use two techniques, the so-called "application of the derivative to the ratio" as well as the "elimination of the momentum in the plateau region" both yielding $F_3(0)$ without any model assumption on its Q^2-dependence.

In order to compute the CP-violating matrix element and extract the CP-odd form factor $F_3(Q^2)$ one needs the evaluation of the topological charge, $\mathcal{Q}$. In this work we employ the field theoretic definition and use cooling and the gradient flow to smooth the gauge links and obtain a well-defined, renormalization-free topological charge [30]. We consider the Wilson, the Symanzik tree-level improved and the Iwasaki actions for the cooling and the gradient flow. Smoothing with different actions leads to observables, such as the nEDM, with potentially different lattice artifacts due to the fact that the topological charge between different actions differs only by lattice artifacts [31]. The results on the nEDM arising from these different definitions of the topological charge are compared and found compatible, demonstrating that lattice artifacts in the definition of the topological charge are small. In Fig. 1 we show our final result for $F_3(0)/(2m_N)$ as well as results from other lattice investigations with dynamical quarks that have been obtained using θ as a real parameter in the QCD Lagrangian keeping the comparison within a similar lattice methodology where lattice systematics are expected to be similar. We note that results obtained using formulations with an imaginary θ such as those

by Guo *et al.* [34] are in agreement with our value. However, in Fig. 1 and in what follows we choose to compare results using a setup with a real value of θ. We also do not show results obtained in the quenched approximation [35]. Our value displayed in Fig. 1 is the weighted average of the values obtained using different methods for extracting $F_3(0)$ (see Section 8), while for the topological charge, we employ the Iwasaki action for its definition, which is the same as the gauge action used in the simulations. For the data shown in Fig. 1 we use gradient flow for the computation of the topological charge, which are, however, equivalent to the ones using cooling results (see Section 7). We also include, for comparison, the value of the nEDM arising from a recent chiral perturbation theory analysis at next to leading order [20].

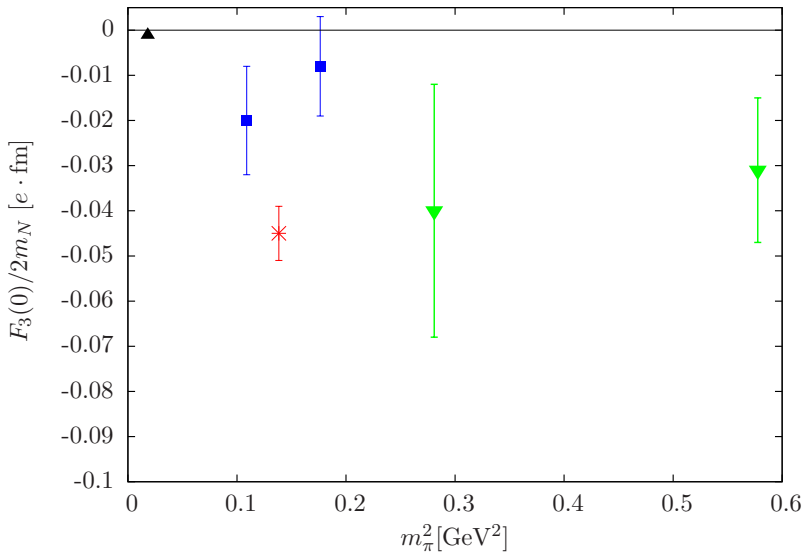

Figure 1: $F_3(0)/(2m_N)$ versus the pion mass squared (m_π^2). Results using N_f=2+1+1 twisted mass fermions (this work) are shown with a red asterisk. We also show results for N_f=2+1 domain wall fermions [32] at $a \simeq 0.11$fm where the CP-odd $F_3(Q^2)$ was evaluated and $F_3(0)$ was determined by fitting its Q^2-dependence (blue squares). Results obtained with N_f=2 Clover fermions at $a \simeq 0.11$fm using a background electric field method are shown with downward green triangles [33]. All errors shown are statistical. A value determined in chiral perturbation theory at next to leading order is shown with the black triangle [20].

The article is organized as follows: In Section 2 we discuss the lattice formulation used for the production of configurations, as well as, the parameters of the ensemble analyzed. Subsequently, in Section 3, we give the decomposition of the nucleon matrix elements in the presence of a CP-violating term in the Lagrangian. In Section 4, Section 5 and Section 6 we explain the computation of correlation functions and the extraction of the form factor $F_3(Q^2)$ in lattice QCD, including the techniques used to obtain $F_3(0)$. In Section 7, we discuss the computation of the topological charge using both the cooling and the gradient flow methods. Finally, in Section 8 we present our results for the nEDM and in Section 9 we provide our conclusions.

2 Simulation

2.1 Formulation

We discuss here the formulation used for the production of the gauge configurations analyzed in this work. For the gluonic action we use the Iwasaki improved action given by [36]

$$S_G = \frac{\beta}{3}\sum_x \left(c_0 \sum_{\substack{\mu,\nu=1 \\ \mu<\nu}}^{4} \left\{1 - \mathrm{ReTr}(U^{1\times 1}_{x,\mu,\nu})\right\} + c_1 \sum_{\substack{\mu,\nu=1 \\ \mu\neq\nu}}^{4} \left\{1 - \mathrm{ReTr}(U^{1\times 2}_{x,\mu,\nu})\right\} \right), \tag{10}$$

where $\beta = 6/g^2$, $U^{1\times 1}_{x,\mu,\nu}$ is the plaquette and $U^{1\times 2}_{x,\mu,\nu}$ rectangular (1×2) Wilson loops. The Symanzik coefficients are set to $c_0 = 3.648$ and $c_1 = -0.331$ and obey the normalization $c_0 + 8c_1 = 1$ ensuring that the Iwasaki action tends to the right Yang-Mills action in the continuum limit. For the discretization of the fermionic action we consider the twisted mass formulation of lattice QCD [37, 38]. Although we are extracting P-odd quantities, all expectation values involve P-even operators and, thus, this formulation provides automatic $O(a)$ improvement at maximal twist [39]. In addition it provides infrared regularization of small eigenvalues and allows for efficient simulations with dynamical fermions. For the mass-degenerate doublet of light quarks we use the action

$$S_F^{(l)}\left[\chi^{(l)}, \overline{\chi}^{(l)}, U\right] = a^4 \sum_x \overline{\chi}^{(l)}(x)\big(D_W[U] + m_{0,l} + i\mu_l\gamma_5\tau^3\big)\chi^{(l)}(x)\,, \tag{11}$$

where τ^3 is the third Pauli matrix acting in the flavour space, $m_{0,l}$ the bare untwisted light quark mass and μ_l the bare twisted light quark mass. The massless Wilson-Dirac operator is given by

$$D_W[U] = \frac{1}{2}\gamma_\mu(\vec{\nabla}_\mu + \vec{\nabla}^*_\mu) - \frac{ar}{2}\vec{\nabla}_\mu\vec{\nabla}^*_\mu\,, \tag{12}$$

with

$$\vec{\nabla}_\mu\psi(x) = \frac{1}{a}\left[U_\mu(x)\psi(x+a\hat{\mu}) - \psi(x)\right] \quad \text{and} \quad \vec{\nabla}^*_\mu\psi(x) = -\frac{1}{a}\left[U^\dagger_\mu(x-a\hat{\mu})\psi(x-a\hat{\mu}) - \psi(x)\right], \tag{13}$$

the forward and backward covariant derivatives, respectively. The action is written in terms of the fields in the "twisted basis", $\chi^{(l)}$, which are related to the fields in the physical basis, $\psi^{(l)}$, at maximal twist through the transformations

$$\psi^{(l)}(x) = \frac{1}{\sqrt{2}}\left(\mathbb{1} + i\tau^3\gamma_5\right)\chi^{(l)}(x), \qquad \text{and} \qquad \overline{\psi}^{(l)}(x) = \overline{\chi}^{(l)}(x)\frac{1}{\sqrt{2}}\left(\mathbb{1} + i\tau^3\gamma_5\right). \tag{14}$$

Apart from the doublet of light quarks, we also include a twisted heavy mass-split doublet $\chi^{(h)} = (\chi_c, \chi_s)$ for the strange and charm quarks [40]. The associated action is

$$S_F^{(h)}\left[\chi^{(h)}, \overline{\chi}^{(h)}, U\right] = a^4 \sum_x \overline{\chi}^{(h)}(x)\big(D_W[U] + m_{0,h} + i\mu_\sigma\gamma_5\tau^1 + \tau^3\mu_\delta\big)\chi^{(h)}(x)\,, \tag{15}$$

with $m_{0,h}$ the bare untwisted quark mass for the heavy doublet, μ_σ the bare twisted mass along the τ^1 direction and μ_δ the mass splitting in the τ^3 direction. The heavy quark fields in the twisted basis are related to those in the physical basis at maximal twist through

$$\psi^{(h)}(x) = \frac{1}{\sqrt{2}}\left(\mathbb{1} + i\tau^1\gamma_5\right)\chi^{(h)}(x), \qquad \text{and} \qquad \overline{\psi}^{(h)}(x) = \overline{\chi}^{(h)}(x)\frac{1}{\sqrt{2}}\left(\mathbb{1} + i\tau^1\gamma_5\right). \tag{16}$$

Unless otherwise stated, in what follows we used the quark fields in the physical basis. The fermionic action in Eq. (11) breaks parity and isospin at non-vanishing lattice spacing with the latter inducing a cut-off effect of $O(a^2)$ [38].

The reader can find more details on the twisted mass fermion action in Ref. [41]. Simulating a charm quark may give rise to concerns regarding cut-off effects. The observables in this work cannot be used to check for finite lattice spacing effects induced by heavy sea quarks. However, analyses in Refs. [42, 43, 44] show that such cut-off effects are small.

2.2 Simulation Details

A number of new techniques are implemented for the extraction of the nEDM using gauge configurations produced with N_f=2+1+1 twisted mass fermions [45]. To explore these techniques we analyze a single ensemble for which a large number of gauge configurations are available allowing us to reach the required accuracy to reliably benchmark the various methods. Although this is a calculation using a single ensemble, previous studies have shown that finite lattice spacing effects on e.g. the nucleon mass for $a < 0.1$ fm are smaller than our statistical errors of about $\sim 3\%$ and we expect this to hold also here. The ensemble is the so called B55.32 in the notation of Ref. [45], which has a lattice spacing of $a \simeq 0.082$ fm determined from the nucleon mass, pion mass 373 MeV, and a spatial lattice extent of $L/a = 32$. The parameters of the ensemble are given in Table 1.

$\beta = 1.95$, $a = 0.0823(10)$ fm, $r_0/a = 5.710(41)$		
$32^3 \times 64$, $L = 2.6$ fm	$a\mu$	0.0055
	No. of confs	4623
	$a\, m_\pi$	0.15518(21)(33)
	Lm_π	4.97
	m_π	0.373 GeV
	am_N	0.5072(17)
	m_N	1.220(5) GeV

Table 1: Input parameters $(\beta, L, a\mu)$ of our lattice calculation (B55.32 ensemble) including the lattice spacing, a, determined from the nucleon mass. Both the neutron (m_N) and pion (m_π) mass are given in lattice and physical units.

3 Nucleon matrix elements in the presence of the θ-term

A precise determination of the neutron electric dipole moment from first principles may provide a valuable input for future experiments seeking to observe a non-vanishing nEDM. It has been recognized since many years that lattice QCD provides an ideal framework for a non-perturbative investigation of the nEDM with first attempts to evaluate it dating back nearly three decades [46]. This first pioneering work was based on the introduction of an external electric field and the measurement of the associated energy shift. Although for the following ten years there was not much progress, during the last decade the study of nEDM has been revived [47, 48, 49, 50, 51, 33, 52] with new approaches being developed. These new methods involve the calculation of the CP-odd $F_3(Q^2)$ form factor by treating the θ-parameter perturbatively [47, 48, 49, 32, 35] or, simulating the theory with an imaginary θ [52, 34]. Alternative definitions of the topological charge were also considered as, for example, replacing the topological charge operator with the flavour-singlet pseudoscalar density employing the axial chiral Ward identities [47, 48].

Despite the recent progress, a lattice determination of the nEDM is inherently difficult and still remains a challenging task. The expectation value of an operator $\mathcal{O}$ in a theory with non-conserving CP-symmetry can, in principle, be obtained by using the path integral formulation, with the Lagrangian given in Eq. (5). Thus, the expectation value is given by

$$\langle \mathcal{O}(x_1, ..., x_n) \rangle_\theta = \frac{1}{Z_\theta} \int d[U] d[\psi_f] d[\bar{\psi}_f]\ \mathcal{O}(x_1, ..., x_n)\ e^{-S_{\rm QCD} + i\theta \int d^4x\, q(x)}\,, \tag{17}$$

where $S_{\rm QCD} = \int d^4x\, \mathcal{L}_{\rm QCD}$ and $\mathcal{L}_{\rm QCD}$ is defined in Eq. (2). In what follows, we will use the notation $\langle \ldots \rangle_\theta$ to indicate expectation values in the CP non-conserving theory, where the Chern-Simons term, $\mathcal{L}_{CS}$, is included. However, the numerical determination of the expectation value given in Eq. (17) suffers from the well-known sign problem due to the imaginary character of $\mathcal{L}_{CS}$. Therefore, it is not feasible to produce gauge

configurations with the Lagrangian density of Eq. (5) and carry out an adequate sampling of the gauge field configuration space. We can overcome this obstacle by treating the Chern-Simons contribution perturbatively assuming that θ is a small parameter

$$e^{i\theta \int d^4x\, q(x)} \equiv e^{i\theta \mathcal{Q}} = 1 + i\theta \mathcal{Q} + O(\theta^2)\,. \tag{18}$$

Thus, to leading order in θ, we obtain

$$\langle \mathcal{O}(x_1, ..., x_n)\rangle_\theta = \langle \mathcal{O}(x_1, ..., x_n)\rangle_{\theta=0} + i\theta \left\langle \mathcal{O}(x_1, ..., x_n) \left(\int d^4x\, q(x) \right) \right\rangle_{\theta=0} + O(\theta^2)\,, \tag{19}$$

where

$$\mathcal{Q} = \int d^4x\, q(x)\,, \tag{20}$$

is the topological charge. This expansion becomes our starting point for the calculation of the CP-odd form factor $F_3(Q^2)$ and, consequently, of the nEDM.

In the remaining part of this section we present the methodology of our work in order to extract F_3, based on the linear response of the CP-violating strength parameter, θ. We adopt the formulation introduced in Ref. [49] as summarized below.

In order to extract the CP-violating electric dipole form factor $F_3(Q^2)$ we consider the nucleon matrix element of the electromagnetic current, given as

$$J^{\rm em}_\mu = \sum_f e_f \bar{\psi}_f \gamma_\mu \psi_f\,, \tag{21}$$

where e_f denotes the electric charge of the quark field ψ_f. The nucleon matrix element of the electromagnetic operator in the θ-vacuum can be written as

$${}_\theta\langle N(\vec{p}_f, s_f)|J^{\rm em}_\mu|N(\vec{p}_i, s_i)\rangle_\theta = \bar{u}^\theta_N(\vec{p}_f, s_f)\, W^\theta_\mu(Q)\, u^\theta_N(\vec{p}_i, s_i)\,, \tag{22}$$

where p_f (p_i) and s_f (s_i) are the momentum and spin of the final (initial) spin-1/2 nucleon state N. According to parity arguments, $W^\theta_\mu(Q)$ is decomposed into an even and an odd part. Up to order θ, this has the form

$$W^\theta_\mu(Q) \quad = \quad W^{\rm even}_\mu(Q) + i\theta\, W^{\rm odd}_\mu(Q)\,. \tag{23}$$

The even part $W^{\rm even}_\mu(Q)$ can be written in terms of the CP-conserving Pauli and Dirac form factors $F_1(Q^2)$ and $F_2(Q^2)$, respectively

$$W^{\rm even}_\mu(Q) = \gamma_\mu F_1(Q^2) - i\,\frac{F_2(Q^2)}{2m_N}\, Q_\nu\, \sigma_{\nu\mu}, \tag{24}$$

while the odd part $W^{\rm odd}_\mu(Q)$ is written in terms of the electric dipole $F_3(Q^2)$ and the anapole $F_A(Q^2)$ form factors

$$W^{\rm odd}_\mu(Q) = -i\,\frac{F_3(Q^2)}{2m_N}\, Q_\nu\, \sigma_{\nu\mu}\gamma_5 + F_A(Q^2)\left(Q_\mu \not{Q} - \gamma_\mu\, Q^2\right)\gamma_5\,. \tag{25}$$

In the absence of the θ-term in the action, only the even part remains. The additional form factors that arise in the odd part for a non-zero value of θ is the CP-violating form factor, $F_3(Q^2)$, which gives the electric dipole moment according to Eq. (9), and the P-violating, but T-preserving, form factor, $F_A(Q^2)$, which measures the anapole moment of the nucleon. Hence, the anapole form factor is C-violating. Since the action is C-preserving such a form-factor is zero and, thus, will not be considered here.

One approach to study the electric dipole moment, is to generate gauge configurations including the θ-term in the action by considering an imaginary θ [34]. We instead use a real value of θ and expand the matrix elements to leading order in θ. This allows us to make use of the gauge configurations generated without the θ-term to evaluate the appropriate expectation values, according to Eq. (19). We first examine the expressions

with the θ-term in the action before we perform the expansion to leading order in θ. We are interested in the three-point function given by

$$G^{\mu,(\theta)}_{3\rm pt}(\vec{q},t_f,t,t_i) \equiv \langle J_N(\vec{p}_f,t_f)\, J^{\rm em}_\mu(\vec{q},t)\, \overline{J}_N(\vec{p}_i,t_i)\rangle_\theta\,, \tag{26}$$

where $\overline{J}_N(\vec{p}_i,t_i)$ and $J_N(\vec{p}_f,t_f)$ are the interpolating operators at the time-space of the source and the sink, respectively. Thus, according to our notation the nucleon is created at time t_i with momentum $\vec{p}_i$, it couples with the electromagnetic current at some later time t, and then is annihilated at time t_f having momentum $\vec{p_f}$. The momentum transfer is thus $\vec{Q}=\vec{q}=\vec{p_f}-\vec{p_i}$. The subscript θ in Eq. (26) implies that the expectation value is taken with respect to the action including the CP-violating term (Eq. (17)).

Inserting complete set of states in the three-point function of Eq. (26) one obtains

$$\begin{aligned} G^{\mu,(\theta)}_{3\rm pt}(\vec{q},t_f,t_i,t) &\simeq e^{-E^f_{N^\theta}(t_f-t)}e^{-E^i_{N^\theta}(t-t_i)} \\ &\times \sum_{s_f,s_i}\langle J_N|N(\vec{p}_f,s_f)\rangle_{\theta\theta}\langle N(\vec{p}_f,s_f)|J^{\rm em}_\mu|N(\vec{p}_i,s_i)\rangle_{\theta\theta}\langle N(\vec{p}_i,s_i)|\overline{J}_N\rangle\,, \end{aligned} \tag{27}$$

with $E^f_{N^\theta}\equiv E^f_{N^\theta}(\vec{p}_f)=\sqrt{\vec{p}_f^{\,2}+m^2_{N^\theta}}$ and $E^i_{N^\theta}\equiv E^i_{N^\theta}(\vec{p}_i)=\sqrt{\vec{p}_i^{\,2}+m^2_{N^\theta}}$. The nucleon states for non-zero θ-term are denoted as $|N\rangle_\theta$, and are normalized as

$$\langle J_N|N(\vec{p},s)\rangle_\theta = Z^\theta_N u^\theta_N(\vec{p},s), \quad \text{and} \quad {}_\theta\langle N(\vec{p},s)|\overline{J}_N\rangle = (Z^\theta_N)^*\,\bar{u}^\theta_N(\vec{p},s)\,. \tag{28}$$

The spinors $u^\theta_N(\vec{p},s)$ and $\bar{u}^\theta_N(\vec{p},s)$ satisfy the Dirac equation

$$\left(i\not{p}+m_{N^\theta}e^{-i2\alpha(\theta)\gamma_5}\right)u^\theta_N(\vec{p},s) = \bar{u}^\theta_N(\vec{p},s)\left(i\not{p}+m_{N^\theta}e^{-i2\alpha(\theta)\gamma_5}\right)=0\,, \tag{29}$$

with the phase $e^{-i2\alpha(\theta)\gamma_5}$ appearing in the mass term due to the CP breaking in the θ-vacuum. This requirement suggests that $\alpha(\theta)$ is odd in θ, while m_{N^θ} and Z^θ_N are even. In the presence of the θ-term, the spinor sum takes a phase in the mass term, becoming

$$\Lambda^{(\theta)}_{1/2}(\vec{p}) = \sum_s u^\theta_N(\vec{p},s)\bar{u}^\theta_N(\vec{p},s) = \frac{-i\not{p}+m_{N^\theta}e^{i2\alpha(\theta)\gamma_5}}{2E_{N^\theta}}\,. \tag{30}$$

For small values of the θ parameter we can expand the above expressions, and to leading order in θ, we obtain

$$\alpha(\theta)=\alpha^1\theta+O(\theta^3), \quad m_{N^\theta}=m_N+O(\theta^2) \quad \text{and} \quad Z^\theta_N=Z_N+O(\theta^2)\,. \tag{31}$$

Upon substituting the above expressions in Eq. (27) one obtains

$$\begin{aligned} G^{\mu,(\theta)}_{3\rm pt}(\vec{q},t_f,t_i,t) &= |Z_N|^2 e^{-E^f_N(t_f-t)}e^{-E^i_N(t-t_i)}\frac{-i\not{p}_f+m_N(1+2i\alpha^1\theta\gamma_5)}{2E^f_N} \\ &\times \left[W^{\rm even}_\mu(Q)+i\theta W^{\rm odd}_\mu(Q)\right]\frac{-i\not{p}_i+m_N(1+2i\alpha^1\theta\gamma_5)}{2E^i_N}+O(\theta^2)\,, \end{aligned} \tag{32}$$

up to linear terms in θ. When combined with the leading order of Eq. (19), the above equation contains all the information needed for the evaluation of $F_3(Q^2)$. The advantage of this method is that the Green's functions of the theory in the presence of the CP-violating term can be expressed in terms of expectation values obtained using the gauge configurations generated with the action with θ set to zero. For the three-point function, this gives

$$G^{\mu,(\theta)}_{3\rm pt}(\vec{q},t_f,t_i,t) = \langle J_N(\vec{p}_f,t_f)J^{\rm em}_\mu(\vec{q},t)\overline{J}_N(\vec{p}_i,t_i)\,\rangle_\theta \tag{33}$$

$$= G^{\mu,(0)}_{3\rm pt}(\vec{q},t_f,t_i,t)+i\,\theta\,G^{\mu,(0)}_{3{\rm pt},\mathcal{Q}}(\vec{q},t_f,t_i,t)+O\left(\theta^2\right), \tag{34}$$

where

$$G^{\mu,(0)}_{\rm 3pt}(\vec{q},t_f,t_i,t) = \langle J_N(\vec{p}_f,t_f) J^{\rm em}_\mu(\vec{q},t) \overline{J}_N(\vec{p}_i,t_i)\rangle, \quad (35)$$

$$G^{\mu,(0)}_{\rm 3pt,\mathcal{Q}}(\vec{q},t_f,t_i,t) = \langle J_N(\vec{p}_f,t_f) J^{\rm em}_\mu(\vec{q},t) \overline{J}_N(\vec{p}_i,t_i)\mathcal{Q}\rangle. \quad (36)$$

We now equate Eq. (34) to Eq. (32) and express $G^{\mu,(0)}_{\rm 3pt}$ and $G^{\mu,(0)}_{\rm 3pt,\mathcal{Q}}$ through the $W^{\rm even}_\mu(Q)$ and $W^{\rm odd}_\mu(Q)$ parts, respectively

$$G^{(0)}_{\rm 3pt}(\vec{q},t_f,t_i,t) = |Z_N|^2 e^{-E^f_N(t_f-t)} e^{-E^i_N(t-t_i)} \frac{-i\not{p}_f + m_N}{2E^f_N} W^{\rm even}_\mu(Q) \frac{-i\not{p}_i + m_N}{2E^i_N}, \quad (37)$$

$$\begin{aligned} G^{(0)}_{\rm 3pt,\mathcal{Q}}(\vec{q},t_f,t_i,t) &= |Z_N|^2 e^{-E^f_N(t_f-t)} e^{-E^i_N(t-t_i)} \Big[\frac{-i\not{p}_f + m_N}{2E^f_N} W^{\rm odd}_\mu(Q) \frac{-i\not{p}_i + m_N}{2E^i_N} \\ &+ \frac{2\alpha^1 m_N}{2E^f_N}\gamma_5 W^{\rm even}_\mu(Q) \frac{-i\not{p}_i + m_N}{2E^i_N} + \frac{-i\not{p}_f + m_N}{2E^f_N} W^{\rm even}_\mu(Q) \frac{2\alpha^1 m_N}{2E^i_N}\gamma_5 \Big]. \end{aligned} \quad (38)$$

A similar analysis can be carried out for the case of the two-point functions. In the presence of the θ-term of Eq. (5) the relevant two-point function is given by

$$G^{(\theta)}_{\rm 2pt}(\vec{q},t_f,t_i) \equiv \langle J_N(\vec{q},t_f)\overline{J}_N(\vec{q},t_i)\rangle_\theta = |Z^\theta_N|^2 e^{-E_{N^\theta}(t_f-t_i)} \frac{-i\not{Q} + m_{N^\theta} e^{i2\alpha(\theta)\gamma_5}}{2E_{N^\theta}}. \quad (39)$$

By treating the Chern-Simons term perturbatively one obtains

$$G^{(\theta)}_{\rm 2pt}(\vec{q},t_f,t_i) = G^{(0)}_{\rm 2pt}(\vec{q},t_f,t_i) + i\,\theta\, G^{(0)}_{\rm 2pt,\mathcal{Q}}(\vec{q},t_f,t_i) + O\left(\theta^2\right), \quad (40)$$

where

$$G^{(0)}_{\rm 2pt}(\vec{q},t_f,t_i) = \langle J_N(\vec{q},t_f)\overline{J}_N(\vec{q},t_i)\rangle = |Z_N|^2 e^{-E_N t} \frac{-i\not{Q} + m_N}{2E_N}, \quad (41)$$

$$G^{(0)}_{\rm 2pt,\mathcal{Q}}(\vec{q},t_f,t_i) = \langle J_N(\vec{q},t_f)\overline{J}_N(\vec{q},t_i)\mathcal{Q}\rangle = |Z_N|^2 e^{-E_N t} \frac{2\alpha^1 m_N}{2E_N}\gamma_5. \quad (42)$$

From the two-point function $G^{(0)}_{\rm 2pt,\mathcal{Q}}$ one can extract the parameter α^1, which enters in the decomposition of the nucleon matrix element to leading order in θ. This will be further discussed in Section 5.

Using Eq. (42) in conjunction with Eqs. (37) and (38) one can obtain $F_3(Q^2)$ from the leading order in θ. To summarize, this approach requires: i) the evaluation of two- and three-point functions using gauge configurations simulated by setting $\theta = 0$, ii) the computation of the topological charge $\mathcal{Q}$ that will be explained in Section 7, and iii) choosing appropriate projectors in order to extract $F_3(Q^2)$ using suitable ratios of correlation functions, as will be explained in Section 6.

4 Correlation functions

Taking into account the Dirac structure of the matrix elements the two- and three-point functions are expressed as

$$G_{2\mathrm{pt}}(\vec{q},t_f,t_i,\Gamma_0) \equiv |Z_N|^2 e^{-E_N(t_f-t_i)} {\Gamma_0}^{\alpha\beta}\Big[\Lambda_{1/2}(\vec{q})\Big]_{\alpha\beta}, \tag{43}$$

$$G_{2\mathrm{pt},\mathcal{Q}}(\vec{q},t_f,t_i,\Gamma_5) \equiv |Z_N|^2 e^{-E_N(t_f-t_i)} {\Gamma_5}^{\alpha\beta}\Big[\frac{\alpha^1 m_N}{E_N}\gamma_5\Big]_{\alpha\beta}, \tag{44}$$

$$G^{\mu}_{3\mathrm{pt}}(\vec{q},t_f,t_i,t,\Gamma_k) = |Z_N|^2 e^{-E^f_N(t_f-t)} e^{-E^i_N(t-t_i)} \Gamma_k^{\alpha\beta}\Big[\Lambda_{1/2}(\vec{p}_f) W^{\mathrm{even}}_{\mu}(Q)\Lambda_{1/2}(\vec{p}_i)\Big]_{\alpha\beta}, \tag{45}$$

$$\begin{aligned} G^{\mu}_{3\mathrm{pt},\mathcal{Q}}(\vec{q},t_f,t_i,t,\Gamma_k) &= |Z_N|^2 e^{-E^f_N(t_f-t)} e^{-E^i_N(t-t_i)} \Gamma_k^{\alpha\beta}\Bigg[\Lambda_{1/2}(\vec{p}_f) W^{\mathrm{odd}}_{\mu}(Q)\Lambda_{1/2}(\vec{p}_i) \\ &+ \frac{\alpha^1 m_N}{E^f_N}\gamma_5 W^{\mathrm{even}}_{\mu}(Q)\Lambda_{1/2}(\vec{p}_i) + \Lambda_{1/2}(\vec{p}_f) W^{\mathrm{even}}_{\mu}(Q)\frac{\alpha^1 m_N}{E^i_N}\gamma_5\Bigg]_{\alpha\beta}. \end{aligned} \tag{46}$$

Note that we dropped the θ-superscript on the two- and three-point functions, since from now on we consider expectation values with $\theta = 0$. Also we define $\Lambda_{1/2}$ that is given in Eq. (30) by setting $\theta = 0$ and Γ_j is an appropriate projector acting on the Dirac structure of the two- and three-point functions. For the three-point function we choose the three projectors given by

$$\Gamma_k = \frac{i}{4}(\mathbb{1} + \gamma_0)\,\gamma_5\,\gamma_k \quad (k = 1,2,3)\,, \tag{47}$$

which can disentangle the four form factors. Using three projectors (one for each spatial direction) instead of summing over k increases the computational cost, since separate sequential inversions are required for each projector. We use inexact deflation [53, 54] to speedup the inversions. In total we do three inversions for the projectors and four for each sink-source time separations. The use of inexact deflation brings a factor of three speedup enabling us to do twelve inversions with the cost of four [55]. The use of the three projectors is needed for the application of the position space methods for the extraction of $F_3(0)$ as discussed in Subsection 6.2.2.

Two projectors are employed in the evaluation of the two-point functions, namely

$$\Gamma_0 = \frac{1}{4}\,(\mathbb{1} + \gamma_0)\,, \quad \Gamma_5 = \frac{\gamma_5}{4}\,, \tag{48}$$

with the projector Γ_5 needed in order to access the parameter α^1.

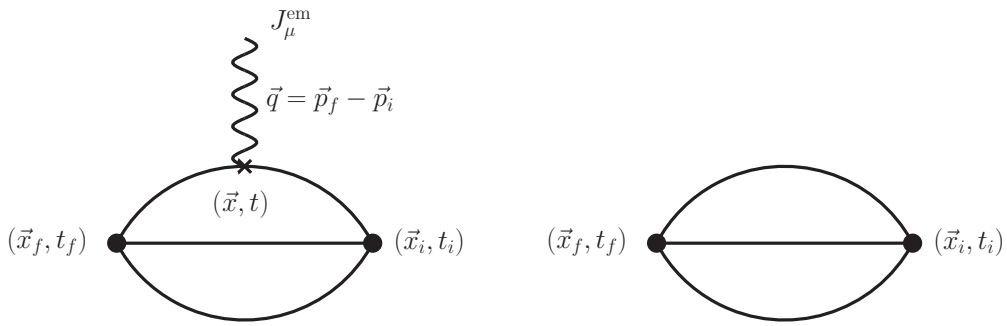

Figure 2: Diagrammatic representation of the connected three-point function (left) and two-point function (right).

In the actual computation, we employ the proton interpolating operators, which in the physical basis reads

$$J_N(x)=\epsilon^{abc}u^a_\alpha \left[u(x)^{\top b}\mathcal{C}\gamma_5 d(x)^c\right] , \tag{49}$$

where $\mathcal{C}$ is the charge conjugation matrix. Since we employ degenerate up and down quarks, the proton Green's functions are equivalent to those of the neutron. Our framework preserves isospin so the proton and neutron electric dipole moments are the same up to a sign. We use Gaussian smeared quark fields [56, 57] to increase the overlap with the neutron state and decrease the overlap with excited states. The smeared interpolating fields are given by

$$\begin{aligned} q^a_{\text{smear}}(t,\vec{x}) &= \sum_{\vec{y}} F^{ab}(\vec{x},\vec{y};U(t))\; q^b(t,\vec{y}) , \\ F &= (\mathbb{1}+a_G H)^{N_G} , \\ H(\vec{x},\vec{y};U(t)) &= \sum_{i=1}^{3}[U_i(x)\delta_{x,y-\hat{\imath}}+U_i^\dagger(x-\hat{\imath})\delta_{x,y+\hat{\imath}}] . \end{aligned} \tag{50}$$

In addition, we apply APE-smearing to the gauge fields U_μ entering the hopping matrix H. The parameters for the Gaussian smearing a_G and N_G are optimized using the nucleon ground state [58]. Different combinations of N_{G} and a_{G}, have been tested in previous work and it was found that combinations of N_G and a_G that give a root mean square radius of about 0.5 fm are optimal for suppressing excited states in the nucleon case. The results of this work have been produced with $N_G = 50$, $a_G = 4$, $N_{\text{APE}} = 20$, $a_{\text{APE}} = 0.5$.

Besides the connected three-point function depicted in Fig. 2 there is a disconnected diagram that can contribute to the nucleon matrix element of the electromagnetic current. However, from a previous study [55], we found for $\sigma_{\pi N}$ a maximum disconnected contribution of about 10% of the connected while for the electromagnetic form factors at the lowest available Q^2 contributions are less than 1%. Hence, although disconnected contributions to F_3 have not yet been studied, we expect them to be of similar magnitude as for the other nucleon form factors. Since the nEDM is a rather noisy observable we neglect the disconnected contribution in the present computation. Hence, the correlators of Eqs. (45) - (46) are calculated using the connected diagram only. For the computation of the connected three-point function we employ sequential inversions through the sink.

In our computation we take the nucleon creation operator at a fixed position $\vec{x}_i = \vec{0}$ (source) with momentum $\vec{p}_i$. The nucleon annihilation operator at a later time t_f (sink) carries zero momentum, i.e. we set $\vec{p}_f = 0$. The electromagnetic current J^{em}_μ couples to a quark at an intermediate time t (insertion) and carries momentum $\vec{q}$ while translation invariance enforces $\vec{q} = -\vec{p}_i$. At a fixed sink-source time separation, $t_{\text{sep}} = t_f - t_i$, we obtain results for all possible momentum transfers and insertion times t with one set of sequential inversions per choice of t_f. We consider three values of t_{sep} in order to check for ground state dominance.

5 Extraction of α^1

The α^1 parameter can be determined from a ratio of two-point functions with the appropriate projectors. Although, there is more than one choice for extracting α^1, we find that the optimal choice with respect to the resulting signal-to-noise ratio is given by

$$\text{R}_{2\text{pt}}(\alpha^1,t_f,t_i) = \frac{G_{2\text{pt},\mathcal{Q}}\,(0,t_f,t_i,\Gamma_5)}{G_{2\text{pt}}\,(0,t_f,t_i,\Gamma_0)} , \tag{51}$$

with the two-point functions defined in Eqs. (43) - (44). For the extraction of α^1 no momentum is required and we thus set $\vec{q} = 0$. By taking the large t_{sep} limit Eq. (51) results in a time-independent quantity (plateau)

$$\Pi_{2\text{pt}}(\alpha^1) = \lim_{t_{\text{sep}}\to\infty} \text{R}_{2\text{pt}}(\alpha^1,t_f,t_i) = \alpha^1 , \tag{52}$$

which can be fitted to a constant yielding α^1. The determination of α^1 requires the evaluation of the topological charge, as indicated by the subscript $\mathcal{Q}$ on the two-point function of Eq. (51). The dependence of α^1 on the definition of $\mathcal{Q}$ is investigated in Section 8.1.

6 Extraction of $F_3(Q^2)$

Before we discuss the calculation of the topological charge $\mathcal{Q}$ needed for both the evaluation of α^1 and $F_3(Q^2)$ we first explain our methods to extract $F_3(Q^2)$ at $Q^2 = 0$ using the three- and two-point functions mentioned in the previous section.

Our calculation proceeds by evaluating the diagrams of Fig. 2. In order to cancel all unknown overlaps and the exponential time dependence we take appropriate ratios using the two- and three-point functions of Eq. (43) and Eq. (46). Specific linear combinations for three-point functions given in Eq. (45) are also constructed in order to eliminate the dominant form factors F_1 and F_2, as explained below. When the insertion-source and sink-insertion time separations are large enough so that contamination from higher excitations is small we obtain a time-independent quantity (plateau) to which we fit to extract $F_3(Q^2)$. The traces of Eqs. (43) - (46) are calculated using Dirac trace algebra, which is implemented with a symbolic analysis package in Mathematica (see, e.g., Ref. [59]). For the evaluation of F_3 we consider the following ratio:

$$\begin{aligned} \mathrm{R}^{\mu}_{3\mathrm{pt},\mathcal{Q}}\left(\vec{q}, t_f, t_i, t, \Gamma_k\right) &= \frac{G^{\mu}_{3\mathrm{pt},\mathcal{Q}}(\vec{q}, t_f, t_i, t, \Gamma_k)}{G_{2\mathrm{pt}}(\vec{q}, t_f - t_i, \Gamma_0)} \\ &\times \sqrt{\frac{G_{2\mathrm{pt}}(\vec{q}, t_f - t, \Gamma_0) G_{2\mathrm{pt}}(\vec{0}, t - t_i, \Gamma_0) G_{2\mathrm{pt}}(\vec{0}, t_f - t_i, \Gamma_0)}{G_{2\mathrm{pt}}(\vec{0}, t_f - t, \Gamma_0) G_{2\mathrm{pt}}(\vec{q}, t - t_i, \Gamma_0) G_{2\mathrm{pt}}(\vec{q}, t_f - t_i, \Gamma_0)}}\,, \end{aligned} \tag{53}$$

for each one of the three projectors given in Eq. (48). For sufficiently large separations $t_f - t$ and $t - t_i$ these ratios become time-independent (plateau region)

$$\Pi^{\mu}_{3\mathrm{pt},\mathcal{Q}}\left(\Gamma_k\right) = \lim_{t_f - t \to \infty} \lim_{t - t_i \to \infty} \mathrm{R}^{\mu}_{3\mathrm{pt},\mathcal{Q}}\left(\vec{q}, t_f, t_i, t, \Gamma_k\right)\,, \tag{54}$$

where μ is the current index. Using Eq. (43) and Eq. (46), carrying out the Dirac algebra and simplifying using our kinematics, we obtain the following expressions:

$$\Pi^{0}_{3\mathrm{pt},\mathcal{Q}}\left(\Gamma_k\right) = i\,C Q_k \left[\frac{\alpha^1 F_1(Q^2)}{2m_N} + \frac{(E_N + 3m_N)\alpha^1 F_2(Q^2)}{4m_N^2} + \frac{(E_N + m_N) F_3(Q^2)}{4m_N^2}\right], \tag{55}$$

$$\begin{aligned} \Pi^{j}_{3\mathrm{pt},\mathcal{Q}}\left(\Gamma_k\right) &= C\left[\frac{(E_N - m_N)\alpha^1 \delta_{k,j} F_1(Q^2)}{2m_N} + \frac{Q_k Q_j F_3(Q^2)}{4m_N^2}\right. \\ &+ \left.\frac{\alpha^1 F_2(Q^2)\left(\left(2E_N m_N - 2m_N^2\right)\delta_{k,j} + Q_k Q_j\right)}{4m_N^2}\right] \quad j = 1, 2, 3\,, \end{aligned} \tag{56}$$

where $C = \sqrt{\frac{2m_N^2}{E_N(E_N + m_N)}}$.

The presence of the CP-even form factors in Eqs. (55) - (56) requires the values of $F_1(Q^2)$ and $F_2(Q^2)$. We can eliminate F_1 and F_2 by substituting them with the appropriate CP-even ratios in large time limit [60]. These ratios are given by

$$Q_i\, F_1(Q^2) = \frac{1}{C(E_N + m_N)}\left[4\,i\,m_N^2\,\Pi^{i}_{3\mathrm{pt}}(\Gamma_0) + m_N\,(E_N - m_N)\,\epsilon^{ijk}\,\Pi^{j}_{3\mathrm{pt}}(\Gamma_k)\right], \tag{57}$$

$$Q_i\, F_2(Q^2) = \frac{1}{C(E_N + m_N)}\left[-4\,i\,m_N^2\,\Pi^{i}_{3\mathrm{pt}}(\Gamma_0) + 2\,m_N^2\,\epsilon^{ijk}\,\Pi^{j}_{3\mathrm{pt}}(\Gamma_k)\right], \tag{58}$$

where a summation over the spatial indices j, k is implied. Thus, we can extract F_3 from the following

combination

$$
\begin{aligned}
Q_i\, F_3(Q^2) \;=\; & \frac{1}{C(E_N+m_N)}\Bigg[4\, m_N^2\, \Pi^0_{3\mathrm{pt},\mathcal{Q}}(\Gamma_i) \\
& -\alpha^1\, 2m_N\left(4\, i\, m_N^3\, \Pi^i_{3\mathrm{pt}}(\Gamma_0) + m_N\,(E_N - m_N)\,\epsilon^{ijk}\,\Pi^j_{3\mathrm{pt}}(\Gamma_k)\right) \\
& -\alpha^1(E_N + 3\, m_N)\left(-4\, i\, m_N^2\, \Pi^i_{3\mathrm{pt}}(\Gamma_0) + 2\, m_N^2\,\epsilon^{ijk}\,\Pi^j_{3\mathrm{pt}}(\Gamma_k)\right)\Bigg]\,, \qquad (59)
\end{aligned}
$$

where, instead of F_1 and F_2, we substitute Eqs. (57) - (58) in Eq. (55) allowing us to extract $F_3(Q^2)$. We first calculate α^1 and then take the linear combination of $\Pi^0_{3\mathrm{pt},\mathcal{Q}}(\Gamma_k)$, $\Pi^i_{3\mathrm{pt}}(\Gamma_0)$ and $\Pi^j_{3\mathrm{pt}}(\Gamma_k)$ from which the plateau value directly yields $Q_i\, F_3(Q^2)$. An analysis using separately the ratios involving F_1, F_2 and F_3 (Eqs. (55), (57), (58)) has also been carried out using singular value decomposition, which gave consistent numerical results for $F_3(Q^2)$. Although both Eqs. (55) - (56) involve F_3, we use Eq. (55), which results in a better signal-to-noise ratio. Moreover, the absence of the momentum factor Q_i in front of F_1 and F_2 in Eq. (56) does not allow the usage of Eq. (57) and Eq. (58) to eliminate them in favor of F_3. The case $j \neq k$ does not allow access to the lowest momentum transfer making the extrapolation to $Q^2 = 0$ less reliable.

A more convenient, but equivalent, procedure is to introduce the electric and magnetic Sachs form factors, G_E and G_M, instead of the Dirac and Pauli. These are related via

$$G_E\left(Q^2\right) = F_1\left(Q^2\right) - \frac{Q^2}{4m_N^2} F_2\left(Q^2\right)\,, \qquad (60)$$

$$G_M\left(Q^2\right) = F_1\left(Q^2\right) + F_2\left(Q^2\right)\,. \qquad (61)$$

Employing an appropriate choice of projectors and insertion indices we find

$$\Pi^j_{3\mathrm{pt}}\left(\Gamma_0\right) = -C\frac{i}{2\, m_N} Q_j G_E\left(Q^2\right)\,, \qquad (62)$$

$$\Pi^j_{3\mathrm{pt}}\left(\Gamma_k\right) = -C\frac{1}{2\, m_N}\epsilon_{jik} Q_i G_M\left(Q^2\right)\,, \qquad (63)$$

with the indices i, j, k being spatial. By combining Eqs. (62) - (63) with Eq. (55) we extract the following linear combination of ratios

$$\Pi^k_{F_3} = -i\Pi^0_{3\mathrm{pt},\mathcal{Q}}(\Gamma_k) + i\,\alpha^1\,\Pi^k_{3\mathrm{pt}}\left(\Gamma_0\right) + \alpha^1\,\frac{1}{2}\sum_{i,j=1}^{3}\epsilon_{jki}\Pi^j_{3\mathrm{pt}}\left(\Gamma_i\right) = \frac{C(E_N+m_N)}{4\, m_N^2}\, Q_k\, F_3(Q^2)\,, \qquad (64)$$

for which the decomposition only depends on the desired form factor $F_3(Q^2)$.

As can be seen from Eq. (55), the appearance of the momentum transfer as a multiplicative factor in front of $F_3(Q^2)$ does not allow the calculation of $F_3(Q^2 = 0)$ directly in momentum space. We explain below three different techniques that allow us to extract $F_3(0)$.

6.1 Extraction of $F_3(0)$ through a dipole fit

The first approach is the commonly used parameterization of the Q^2-dependence of $F_3(Q^2)$ extracted from Eq. (55) followed by a fit to extract $F_3(0)$ treating it as a fitting parameter. We use a dipole Ansatz [35] for Q^2-dependence of $F_3(Q^2)$ of the form

$$F_3\left(Q^2\right) = \frac{F_3(0)}{\left(1 + \dfrac{Q^2}{m^2_{F_3}}\right)^2}\,, \qquad (65)$$

where $F_3\left(0\right)$ and m_{F_3} are fit parameters.

6.2 Position space methods

The other approach that was recently developed and applied in the study of the Pauli form factor $F_2(Q^2)$ [29] is based on removing the momentum factor in front of $F_3(Q^2)$ by employing the so called position space methods. There are two ways to accomplish this: the first is to apply a continuum-like derivative to the ratio and the second is to first determine the plateau values in momentum space, then take the Fourier transform to coordinate space and finally transform back to momentum space using a continuous Fourier transform in such a way that the hindering momentum factor is avoided in the final result. In what follows we will refer to first position space method as "application of the derivative to the ratio" whereas to the second as "elimination of the momentum in the plateau region". We briefly explain these techniques in the next two subsections.

6.2.1 Application of the derivative to the ratio technique

Assuming continuous momenta one can formally remove the Q_k dependence in front of $F_3(Q^2)$ in Eq. (64) by applying a derivative with respect to Q_j

$$\lim_{Q^2\to 0}\frac{\partial}{\partial Q_j}\Pi^k_{F_3}(\vec{Q}) = \frac{C\,(E_N+m_N)}{4m_N^2}\delta_{kj}F_3(0)\,. \tag{66}$$

For simplicity we explicitly show the application of the derivative to the ratio in Eq. (53), which leads to the first term in Eq. (64); the generalization on the other two ratios is straightforward. This gives

$$\begin{aligned}\lim_{Q^2\to 0}\frac{\partial}{\partial Q_j}\mathrm{R}^{\mu}_{3\mathrm{pt},\mathcal{Q}}\left(\vec{q},t_f,t_i,t,\Gamma_k\right) &= \lim_{Q^2\to 0}\frac{\frac{\partial}{\partial Q_j}G^{\mu}_{3\mathrm{pt},\mathcal{Q}}(\vec{q},t_f,t_i,t,\Gamma_k)}{G_{2\mathrm{pt}}(\vec{q},t_f,t_i,\Gamma_0)}\,, &(67)\\ &= \frac{1}{G_{2\mathrm{pt}}(\vec{0},t_f,t_i,\Gamma_0)}\cdot\sum_{x_j=-L/2+a}^{L/2-a}\left(\sum_{\substack{x_i=0\\ i\neq j}}^{L-a} i x_j G^{\mu}_{3\mathrm{pt},\mathcal{Q}}(\vec{x},t_f,t_i,t,\Gamma_k)\right), &(68)\end{aligned}$$

where in the second line the three-point function $G^{\mu}_{3\mathrm{pt},\mathcal{Q}}(\vec{x},t_f,t_i,t,\Gamma_k)$ is expressed in position space. The derivative only acts on the three-point function since any derivatives acting on the two-point functions in the above expression vanish exactly when setting $Q^2=0$. In finite volume this expression approximates the derivative of a δ-distribution in momentum space,

$$\begin{aligned}a^3\sum_{x_j=-L/2+a}^{L/2-a}\left(\sum_{\substack{x_i=0\\ i\neq j}}^{L-a} i x_j G^{\mu}_{3\mathrm{pt},\mathcal{Q}}(\vec{x},t_f,t_i,t,\Gamma_k)\right) &= \frac{1}{V}\sum_{\vec{k}}\left(a^3\sum_{x_j=-L/2+a}^{L/2-a}\left(\sum_{\substack{x_i=0\\ i\neq j}}^{L-a} i x_j \exp\left(i\vec{k}\vec{x}\right)\right)\right) G^{\mu}_{3\mathrm{pt},\mathcal{Q}}(\vec{k},t_f,t_i,t,\Gamma_k)\,,\\ &\overset{L\to\infty}{\longrightarrow}\frac{1}{(2\pi)^3}\int d^3\vec{k}\,\frac{\partial}{\partial k_j}\delta^{(3)}(\vec{k})\,G^{\mu}_{3\mathrm{pt},\mathcal{Q}}(\vec{k},t_f,t_i,t,\Gamma_k). &(69)\end{aligned}$$

For finite L this implies a residual t-dependence $G^{\mu}_{3\mathrm{pt},\mathcal{Q}}(\vec{q},t_f,t_i,t,\Gamma_k)\sim\exp\left(-\Delta E_N t\right)$ with $\Delta E_N = E_N\left(\vec{q}\right)-m_N$. Only for $L\to\infty$ we have $\Delta E_N\to 0$.

According to the above formulation, the basic building blocks for this technique are the standard two-point functions and the derivative-like three point functions $\partial G^{\mu}_{3\mathrm{pt},\mathcal{Q}}(\vec{q},t_f,t_i,t,\Gamma_k)/\partial Q_j$. In the actual lattice computation this involves the calculation of the full three-point function in position space before multiplying by x_j, taking the Fourier transformation and forming the ratio of Eq. (68). Additionally, this technique requires a large enough lattice extent L for the summation in Eq. (69) to approximate the δ-function.

In order to extract $F_3(0)$ from the decomposition in Eq. (64) one performs the derivative on the other two three-point functions following the same procedure as outlined above. Namely, one needs the derivatives $\partial G^{\mu}_{3\mathrm{pt},\mathcal{Q}}(\vec{q},t_f,t_i,t,\Gamma_k)/\partial Q_j$, $\partial G^{k}_{3\mathrm{pt}}(\vec{q},t_f,t_i,t,\Gamma_0)/\partial Q_j$ as well as $\partial G^{k}_{3\mathrm{pt}}(\vec{q},t_f,t_i,t,\Gamma_i)/\partial Q_j$. The residual t-dependence that may remain in Eq. (66) of the form $\exp\left(-\Delta E_N t\right)$ is expected to vanish only as $L\to\infty$.

6.2.2 The elimination of the momentum in the plateau region technique

This method was originally developed for the nucleon isovector magnetic moment or equivalently $F_2(0)$ [29] and allows to extract $F_3(0)$ in a model-independent way without the residual time dependence of the previous method. In principle, it is not restricted to the case of a simple momentum prefactor, but can be used to remove any kinematic structure that would otherwise prevent the extraction of a form factor at zero momentum without making a fit Ansatz. In the following we discuss the application of this method for $F_3(0)$. We want to stress that a key element in the extraction of $F_3(Q^2)$ using this method is the use of the projectors of Eq. (47) without summing over the index k.

Our starting point is Eq. (64) which as explained is obtained by combining the corresponding expression for the CP-odd ratio in Eq. (55) with Eqs. (62) - (63). As far as the Q_k-dependence is concerned Eq. (64) is now similar to the one for the magnetic form factor in Eq. (63). Therefore, we adopt the elimination of the momentum in the plateau region technique as discussed in Ref. [29] for this particular linear combination of ratios to obtain a continuous curve for $F_3(Q^2)$ from which the value of $F_3(0)$, and consequently the nEDM, can be extracted. In the following we briefly outline the basic idea behind the elimination of the momentum in the plateau region technique referring the reader to Ref. [61] for more details.

While for the application of the derivative to the ratio approach the time-dependence is only fitted after applying the derivative in position space, the elimination of the momentum in the plateau region technique aims at removing any time-dependence before applying the derivative. For now we restrict ourselves to on-axis momenta, e.g. $\vec{q} = (\pm Q_1, 0, 0)^T$ (and all permutations thereof). After forming the combination of ratios in Eq. (64) we average over all momentum directions taking only index combinations into account that give a non-zero contribution for a given Q_1-value. The resulting, averaged ratios are denoted by $\Pi(Q_1)$.

Applying a Fourier transform on $\Pi(Q_1)$ gives the corresponding ratio $\Pi(y)$ in position space, which satisfies $\Pi(y) \approx -\Pi(-y)$ up to statistical fluctuations. Note that in an actual lattice simulation the Fourier transform requires an additional cutoff $Q_{1\,\mathrm{max}}$, because the calculation of $\Pi(Q_1)$ will be restricted to a limited number of lattice momenta due to noise. Typically this cutoff is much smaller than the maximally allowed lattice momentum. Since we have

$$\Pi(y) = \begin{cases} +\Pi(n), & n = 0, ..., N/2\,, \\ -\Pi(N-n), & n = N/2+1, ..., N-1,\ N = L/a\,, \end{cases} \tag{70}$$

where $n = y/a$, we can average over positive and negative values of y, yielding an exactly antisymmetric expression $\overline{\Pi}(n)$. The most crucial part of this method is to transform $\overline{\Pi}(n)$ back in a way that allows to introduce continuous momenta. This can be achieved by rewriting the corresponding Fourier transform in the following way

$$\begin{aligned} \Pi(k) &= \big[\exp(ikn)\overline{\Pi}(n)\big]_{n=0,\,N/2} + \sum_{n=1}^{N/2-1} \exp(ikn)\overline{\Pi}(n) + \sum_{n=N-1}^{N/2+1} \exp(ik(N-n))\overline{\Pi}(n)\,, \\ &= \big[\exp(ikn)\overline{\Pi}(n)\big]_{n=0,\,N/2} + 2i \sum_{n=1}^{N/2-1} \overline{\Pi}(n) \sin\left(\frac{k}{2}\cdot(2n)\right)\,, \end{aligned} \tag{71}$$

and defining $\hat{k} \equiv 2\sin\big(\frac{k}{2}\big)$ and $P_n\big(\hat{k}^2\big) = P_n\big(\big(2\sin\big(\frac{k}{2}\big)\big)^2\big) = \sin(nk)/\sin\big(\frac{k}{2}\big)$, leading to

$$\Pi(\hat{k}) - \Pi(0) = i \sum_{n=1}^{N/2-1} \hat{k}\, P_n\left(\hat{k}^2\right)\overline{\Pi}(n)\,. \tag{72}$$

The function $P_n\left(\hat{k}^2\right)$ is related to Chebyshev polynomials of the second kind and hence analytic in $(-\infty, +1)$, allowing to evaluate $\Pi(\hat{k})$ at any intermediate value. Dropping the factor $\hat{k}$ in the above expression, we obtain the desired expression for the neutron electric dipole form factor without explicit momentum factors

$$\frac{F_3(\hat{k}^2)}{2m_N} = i \sum_{n=1}^{N/2-1} P_n(\hat{k}^2)\,\overline{\Pi}(n)\,, \tag{73}$$

where we assume that all suppressed kinematic factors have been included in $\overline{\Pi}(n)$. This expression can be computed exactly on the lattice – up to the aforementioned, additional cutoff in the initial Fourier transform – for any reasonable value of $\hat{k}^2$, resulting in a smooth curve for $F_3(Q^2)$. Consequently, taking the statistical errors of the input data into account via resampling yields a smooth error band for the form factor, as we will demonstrate in Section 8.2.3.

It is now straightforward to extend the approach to arbitrary sets of off-axis momentum classes

$$M(Q_1, Q_{\text{off}}^2) = \left\{ \vec{q} \mid \vec{q} = \{\pm Q_1, Q_2, Q_3\},\ Q_2^2 + Q_3^2 = Q_{\text{off}}^2 \right\}, \tag{74}$$

where $\{\pm Q_1, Q_2, Q_3\}$ denotes all permutations of $\pm Q_1$, Q_2 and Q_3. However, to combine the results for $F_3(Q^2)$ for different Q_{off}^2–classes as a function of continuous Euclidean momenta $Q^2 = Q^2(\hat{k}, Q_{\text{off}}^2)$ we need to consider an analytic continuation for classes with $Q_{\text{off}}^2 > 0$ to reach zero total momentum, i.e. $Q^2 = 0$. For our case this amounts to replacing $k \to i\kappa$ and $\hat{k} \to i\hat{\kappa} = -2\sinh\left(\frac{\kappa}{2}\right)$ in the derivation outlined above. Note that this also affects P_n, i.e. $P_n\left(\hat{\kappa}^2\right) = \sinh(n\kappa)/\sinh\left(\frac{\kappa}{2}\right)$. In order to obtain the final result we combine the results from several sets of momentum classes $M(Q_1, Q_{\text{off}}^2)$ by taking the error weighted average of the separate results.

Finally, we remark that in principle Eq. (56) could also be used instead of (55) to calculate $F_3(0)$. However, in this case, not all of the terms share the same momentum prefactor and one expects the signal from this decomposition to be weaker than the one from Eq. (55) due to the additional momentum prefactor for $F_3(Q^2)$. Moreover, from a technical point of view the removal of the double momentum factor $Q_j Q_k$ is more involved. Therefore, we restrict ourselves to the combination of current and projection indices given in Eq. (55).

7 The topological Charge

As already demonstrated in the previous section the evaluation of the $F_3(Q^2)$ form factor requires the computation of the topological charge, $\mathcal{Q}$ defined in Eq. (20). In practice, any valid lattice discretization of $q(x)$ leading to the right continuum expression of the charge density given in Eq. (4) could be used for the evaluation of $\mathcal{Q}$ on the lattice. Here we choose an improved definition:

$$q(x) = c_0 q_L^{\text{clov}}(x) + c_1 q_L^{\text{rect}}(x), \tag{75}$$

with

$$q_L^{\text{clov}}(x) = \frac{1}{32\pi^2}\epsilon_{\mu\nu\rho\sigma}\text{Tr}\left(C_{\mu\nu}^{\text{clov}} C_{\rho\sigma}^{\text{clov}}\right) \quad \text{and} \quad q_L^{\text{rect}}(x) = \frac{2}{32\pi^2}\epsilon_{\mu\nu\rho\sigma}\text{Tr}\left(C_{\mu\nu}^{\text{rect}} C_{\rho\sigma}^{\text{rect}}\right), \tag{76}$$

where

$$C_{\mu\nu}^{\text{clov}}(x) = \frac{1}{4}\text{Im}\left(\quad\right) \quad \text{and} \quad C_{\mu\nu}^{\text{rect}}(x) = \frac{1}{8}\text{Im}\left(\quad + \quad\right). \tag{77}$$

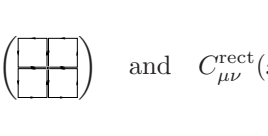

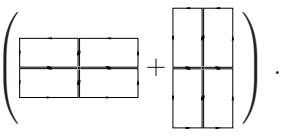

In order to remove the discretization error at tree-level, we use the coefficients $c_0 = 5/3$ and $c_1 = -1/12$. The lattice operator used for the evaluation of the topological charge on thermalized configurations suffers from ultraviolet fluctuations of the gauge configurations, hence leading to non-integer results. It is thus customary to use a smoothing technique, which damps these fluctuations by minimizing the action locally, without destroying the underlying topological structure.

Such techniques include cooling and the more recently introduced gradient flow [62, 30]. It was shown recently [63] that both techniques provide similar results on topological observables such as the average action and the topological susceptibility when smoothing is done with the ordinary Wilson action. In Ref. [31] we show that this is also true for actions that include a rectangular term such as the Iwasaki and the Symanzik tree-level improved action. The equivalence is realized by the leading order perturbative rescaling [31]

$$\tau \simeq \frac{n_c}{3 - 15c_1}, \tag{78}$$

where τ, the gradient flow time, and n_c, the number of cooling steps, are the smoothing scales for gradient flow and cooling, respectively.

We apply both techniques, namely cooling and gradient flow, on the configurations of the B55.32 ensemble using the naive Wilson, the Symanzik tree-level improved and the Iwasaki actions. Regarding the gradient flow we investigate how the elementary integration step ϵ affects our results and find that setting $\epsilon = 0.02$ is a safe option; as a matter of fact we observe that smaller elementary integration steps give indistinguishable results.

While cooling, we measure the improved definition of the topological charge for every cooling step. Since the gradient flow is more expensive, we avoid taking measurements for every integration step, but instead we compute the topological charge every $\Delta\tau = 0.1$; this corresponds to five integration steps. We cover in total $80 - 100$ cooling steps while for gradient flow we fix the maximum gradient flow time according to the perturbative expression of Eq. (78) taking for n_c the maximum number of cooling steps. The cooling/gradient flow rescaling factors are given in Table 2.

Smoothing action	c_0	c_1	n_c/τ	$n_c\,(\sqrt{8t} \approx 0.6\text{fm})$	$\tau\,(n_c)$
Wilson	1	0	3	20	6.7
Symanzik tree-level improved	$\frac{5}{3}$	$-\frac{1}{12}$	4.25	30	7.1
Iwasaki	3.648	-0.331	7.965	50	6.3

Table 2: The first and second columns give the values of the parameter c_0 and c_1 entering in gauge action and the third gives the ratio for n_c/τ extracted using Eq. (78). The fourth column gives the leading order perturbative rescaling between the number of cooling steps and the gradient flow time such that the two smoothing techniques are equivalent, the fifth column gives the value of the cooling step which corresponds to fixing $\sqrt{8t} \approx 0.6$ fm, and the sixth column the associated gradient flow time.

According to Ref. [30] one reads an observable, whose value depends on the topological charge, at a fixed value of $\sqrt{8t} = O(0.1\,\text{fm})$. The gradient-flow time t is chosen such that it is large enough so the relevant observable has small discretization effects but at the same time small enough so that the topological content of the fields is preserved. The observable under consideration here is $F_3/2m_N$ and it should be scale invariant and, thus, show a plateau as a function of τ and n_c at the fixed value of $\sqrt{8t}$ being within the plateau region. For practical reasons we choose a value of τ that satisfies $\sqrt{8t} \approx 0.6$fm and corresponds to the rounded value of n_c taken in steps of ten; the associated values of n_c as well as τ can be found in Table 2. In Ref. [31] we demonstrate in more details that topological quantities on the same ensemble, for the three smoothing actions, become equal after a small number of n_c and the equivalent gradient flow time; as a matter of fact for $\sqrt{8t} \approx 0.6$fm the equality between the smoothing procedures of the gradient flow and cooling is satisfied. In Fig. 3 we present the time history of the topological charge $\mathcal{Q}$ obtained with cooling using $n_c = 50$ and the gradient flow at $\tau = 6.3$ using the Iwasaki action. This plot demonstrates that the topological charge does not suffer from large autocorrelations along the sampling time line with integrated autocorrelation time of $\tau_{\text{int}} = 2.6(1)$ and there is a high correlation of 94% [31] between results obtained using cooling and the gradient flow. The latter is a result of the equivalence between the two procedures. Additionally, in Fig. 3, we provide the associated histograms of the topological charge for both cooling and gradient flow, which is found to be approximately Gaussian (according to Anderson-Darling test [64]). These observations suggest that for both smoothing approaches the sampling of the topological charge is adequately good. Similar results are also obtained for the Wilson and Symanzik tree-level improved actions. These are the basic requirements that the topological charge should obey in order to give reliable results for the nEDM.

8 Results

In this section, we present our results on the CP-odd form factor $\lim_{Q^2\to 0} F_3(Q^2)$ with our main focus being the extraction of the nEDM, using the three approaches discussed in Section 6. Namely we use a dipole Ansatz

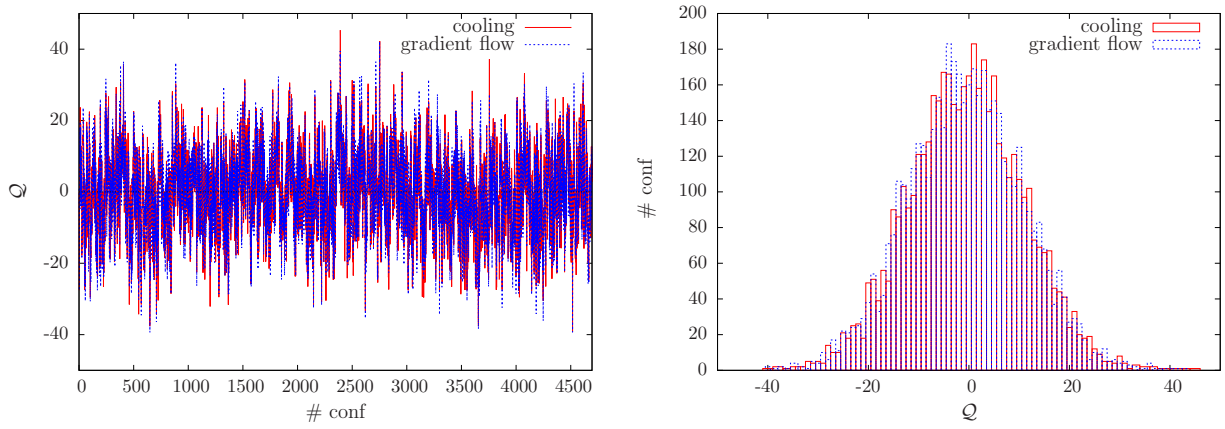

Figure 3: The time history of the topological charge (left panel) and its associated distribution (right panel). The charge has been obtained via cooling (red) and gradient flow (blue) with Iwasaki action with black $n_c = 50$ and $\tau = 6.3$, respectively.

to perform an extrapolation to $Q^2 = 0$, as well as, the two position space techniques. For all three approaches we need the evaluation of α^1, which enters in the determination of $F_3(0)$, as shown in Eq. (64). Hence, we first discuss the determination of α^1.

8.1 Calculation of α^1

To extract α^1 we calculate the two-point function $G_{2\mathrm{pt},\mathcal{Q}}(\vec{q}, t_f, \Gamma_5)$, which involves the topological charge $\mathcal{Q}$, as well as the usual two-point function $G_{2\mathrm{pt}}(\vec{q}, t_f, \Gamma_0)$. Note that the argument t_i has been omitted, since in our calculation we shift the source point to $t_i = 0$. We form the ratio of these two-point functions according to Eq. (51) at zero momentum transfer, $\vec{q} = \vec{0}$. The topological charge is computed using both cooling and the gradient flow method employing the three gauge actions, Wilson, Symanzik tree-level improved and Iwasaki. For the calculation of the α^1 parameter we use a large statistical sample of a total of 36720 two-point functions (2295 configurations, each with 16 source positions). This allows us to decrease significantly the statistical errors on α^1. As a consequence, the bins on which α^1 is computed, do not coincide with those of F_3, and thus we need an alternative procedure to jack-knife for the computation of the statistical errors on the nEDM. This will be discussed in Subsection 8.2.

The ratio $\mathrm{R}_{2\mathrm{pt}}(\alpha^1, t_f)$ is shown in Fig. 4 as a function of t_f/a, for which the topological charge is measured using the gradient flow with the Iwasaki action at $\tau = 6.3$. As can be seen, for $t_f/a > 8$ the ratio becomes time-independent yielding $\Pi_{2\mathrm{pt}}(\alpha^1)$. By fitting to a constant in the plateau region within the time interval 9-20 we extract the value of $\alpha^1 = -0.217(18)$. We have checked that by modifying both the starting and ending time-slices in the fit within the region $t_f/a = 7$ to 22 we get compatible results. An example is shown in Fig. 4 for the range $t_f/a = 10$ to 17, which gives the green band.

The final result on α^1 should not depend on the smoothing scale; in other words there should be a plateau for some region of the smoothing scale n_c or equivalently τ. This is demonstrated in Fig. 5 where we plot the value of α^1 as a function of n_c and the gradient flow time τ rescaled according to Eq. (78) for all three gauge actions. As can be seen, the α^1 parameter remains unchanged after $n_c \geq 20$ cooling steps or the equivalent gradient flow time τ. This is in perfect agreement with fixing $\sqrt{8t} \approx 0.6$fm. Therefore, setting n_c according to the fifth column in Table 2 or fixing to the corresponding flow time for the gradient flow both yield a consistent value for α^1. We will employ the value $\alpha^1 = -0.217(18)$, obtained using the gradient flow at $\tau = 6.3$ for the Iwasaki action in order to determine $F_3(Q^2)$. We also observe that for all gauge actions the value of α^1 extracted when using cooling or the gradient flow to determine the topological charge are

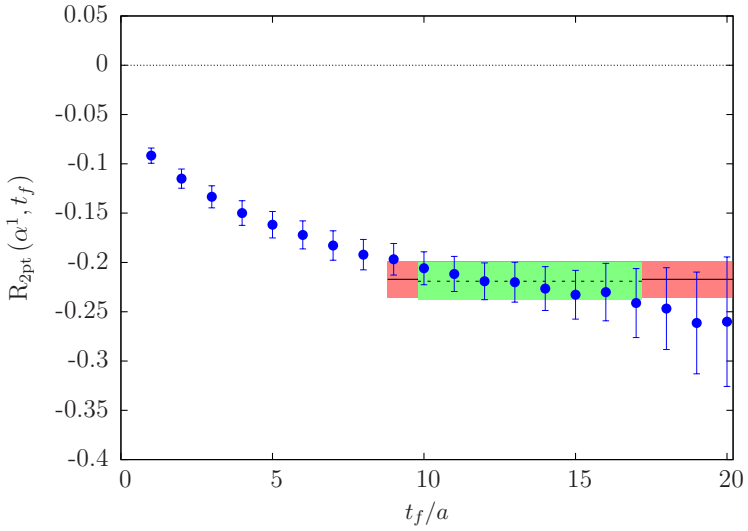

Figure 4: The ratio $R_{2pt}(\alpha^1, t_f)$ as a function of t_f/a (t_i was set to 0). A constant fit between the time-slices 9-20 gives the solid line $\alpha^1 = -0.217(18)$ with $\chi^2/\text{DOF} = 0.51$ and the red band is the associated statistical uncertainty. The green band corresponds to the fit range 10-17 with $\chi^2/\text{DOF} = 0.29$, which is fully compatible with the red one. The employed topological charge $\mathcal{Q}$ is extracted via the gradient flow at $\tau = 6.3$ using the Iwasaki action.

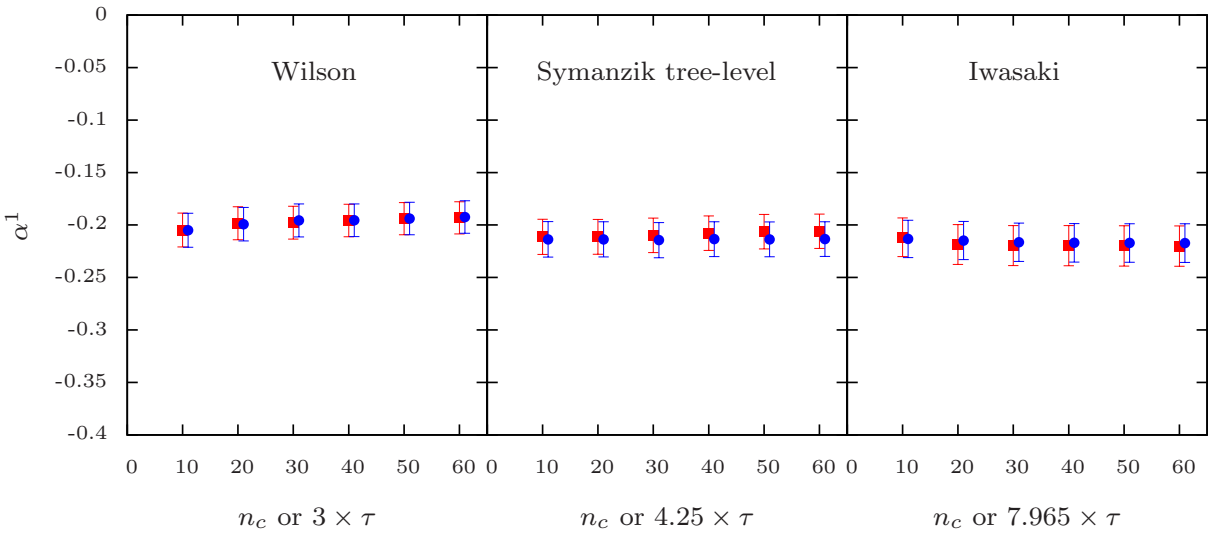

Figure 5: The value of α^1 as a function of n_c or $3 \times \tau$ (left), $4.25 \times \tau$ (center) and $7.965 \times \tau$ (right) for Wilson, Symanzik tree-level improved and Iwasaki smoothing actions, respectively. Data obtained by cooling are shown by the red squares, while data extracted via the gradient-flow are shown by the blue circles and have been shifted horizontally to be more visible.

in agreement, reflecting the equivalence between the two procedures. The results shown in Fig. 5 use the topological charge obtained for every $\Delta n_c = 10$ starting from $n_c = 10$ while cooling and for the corresponding gradient flow time τ when smoothing via the gradient flow. The same computation of the topological charge

is also used in the evaluation of the three-point function. For the determination of the errors we use jack-knife with bin size of 5; larger bin sizes give consistent results.

8.2 Results for $F_3(0)$

8.2.1 $F_3(0)$ via extrapolation in Q^2

We first discuss the determination of $F_3(0)$ extracted by fitting the Q^2-dependence of $F_3(Q^2)$ to the dipole Ansatz given in Eq. (65). $F_3(Q^2)$ has been computed for a sequence of values of the momentum transfers, $Q^2 = 2m_N\sqrt{E_N - m_N}$, with the momentum chosen such that the spatial components Q_i take all possible combinations of $Q_i/(2\pi/L) \in [0, \pm 4]$ (and all permutations thereof). We perform the calculation at three values of the source-sink separation namely $t_{\rm sep} = 10a$, $t_{\rm sep} = 12a$ and $t_{\rm sep} = 14a$ with the statistics being 2357 for $t_{\rm sep} = 10a$, and 4623 for $t_{\rm sep} = 12a, 14a$.

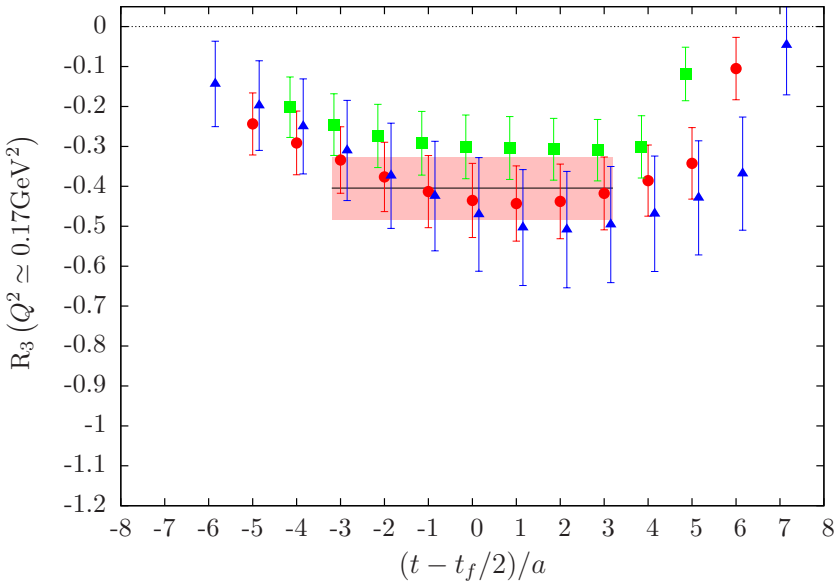

Figure 6: The ratio leading to F_3 (Eq. (64)) for the first non-zero momentum transfer ($Q^2 \simeq 0.17\,\mathrm{GeV}^2$) as a function of the insertion time $(t - t_f/2)/a$. Green squares, red circles and blue triangles correspond to source-sink separation of $t_f/a = 10$, 12, 14, respectively. The topological charge is evaluated using the gradient flow at $\tau = 6.3$ with the Iwasaki action.

In Fig. 6 we show the results for the combination of ratios leading to the extraction of $F_3(Q^2)$ according to Eq. (64). The ratio of F_3 is plotted for three source-sink time separations: $10a$, $12a$, $14a$ corresponding to 0.82, 1.0, 1.15 fm, respectively. As can be seen the results at the three sink-source time separations are consistent. The ratio shown corresponds to the lowest non-zero momentum transfer, that is $Q^2 \simeq 0.17\,\mathrm{GeV}^2$, upon averaging over the data for the two spatial components $Q_i/(2\pi/L) = (\pm 1, 0, 0)$ and three permutations. In what follows we will use $t_{\rm sep} = 12a$, which yields a better statistical accuracy and it is fully consistent with the results obtained for $t_{\rm sep} = 14a$. For $t_{\rm sep} = 12a$, a plateau can be identified in the range $t/a \in [3, 9]$, from which we extract $F_3(Q^2 \simeq 0.17\mathrm{GeV}^2)$ (solid line in Fig. 6). However, for a proper computation of the error we cannot use jackknife since, as mentioned in Section 8.1, the α^1 parameter is computed on 2295 configurations with multiple source positions, while F_3 is computed using 4623 configurations with a single source position, which does not allow to combine the bin values of α^1 and F_3. We thus use the following procedure to take into account the statistical error of α^1 in the evaluation of the error on F_3: We first compute F_3 and the associated jackknife error, dF_3 by employing the mean value for α^1. We then recompute F_3 using $\alpha^1_{\rm max} = \alpha^1 + d\alpha^1$, where

$d\alpha^1$ is the jackknife error of α^1. We denoted the difference in the values obtained using the mean value of α^1 and $\alpha^1_{\rm max}$ by ΔF_3. The final error on F_3 is computed by combining ΔF_3 due to the variation in α^1 with the jackknife error dF_3 in quadrature, namely $\sqrt{(\Delta F_3)^2 + (dF_3)^2}$. In Fig. 6 we show the final error on F_3 with a red band. This procedure of taking into account the error on the α^1 parameter is compatible with the error using a resampling procedure. For the latter we first generate samples for α^1 that are gaussian distributed with $\sqrt{N_s - 1}\, d\alpha^1$, where N_s denotes the number of jackknife samples in our analysis. These samples are then used in our jackknife analysis together with the actual jackknife samples for the remaining quantities.

Once again, we stress that no separate calculation of $F_1(Q^2)$ and $F_2(Q^2)$ is needed, since $F_3(Q^2)$ is extracted from a combination of ratios leading to Eq. (64), upon substituting the expressions for $G_E(Q^2)$ and $G_M(Q^2)$ (Eq. (62) and Eq. (63)) at the level of the time-dependent ratios. In addition, the value of the nucleon mass, m_N, enters in Eq. (64), which is calculated using the nucleon two-point function on the same configurations analyzed for $F_3(Q^2)$ and in the same bin. The value of am_N in lattice units is presented in Table 1.

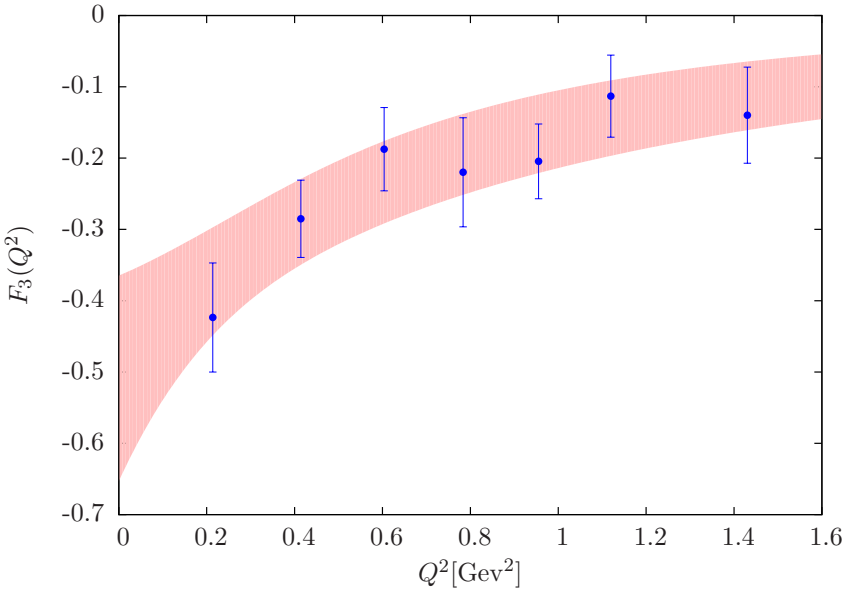

Figure 7: $F_3(Q^2)$ versus Q^2 for the same parameters as in Fig. 6 for $t_{\rm sep} = 12a$. The band is the resulting dipole fit using the form given in Eq. (65) to $F_3(Q^2)$ and data for $Q^2 < 1$ GeV^2. The fit gives $F_3(0) = -0.509(144)$, $am_{F_3} = 0.469(133)$ with $\chi^2/{\rm DOF} = 0.54$.

After determining $F_3(Q^2)$ by identifying the corresponding plateau at each value of Q^2 we perform a fit using the dipole form of Eq. (65), treating $F_3(0)$ as a fitting parameter. In Fig. 7 we show the resulting fit when the Iwasaki smoothing action and gradient flow with $\tau = 6.3$ are used in the calculation of the topological charge. The fit is performed for $Q^2 < 1\,{\rm GeV}^2$. To check for fit stability we vary the upper limit of the fit range, $Q^2_{\rm max}$, from 0.8 to 1.5 GeV^2, and found consistent results for $F_3(0)$.

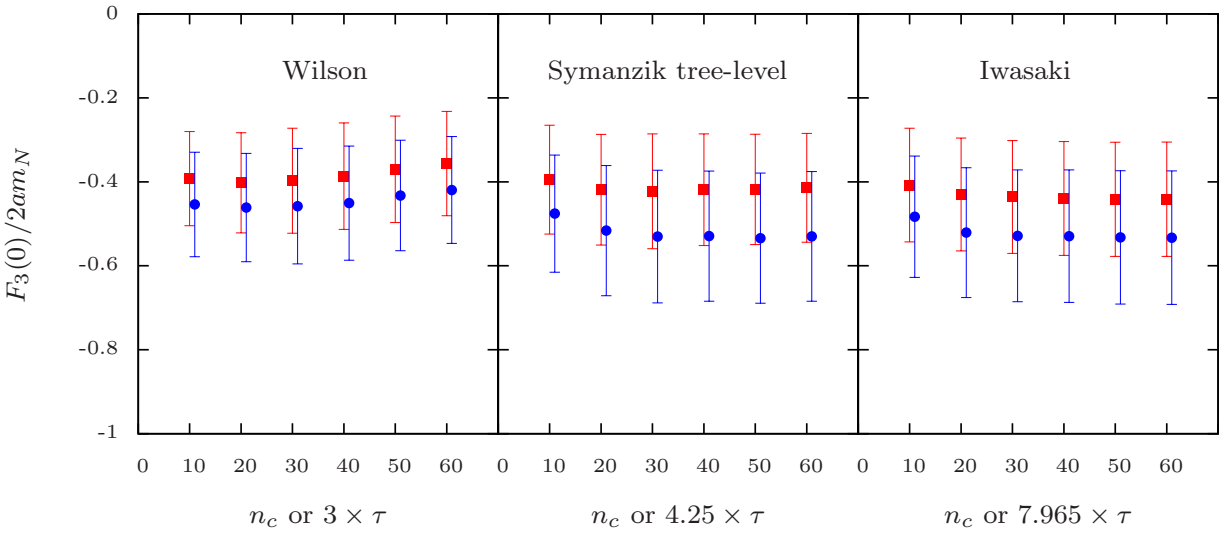

Figure 8: The nEDM in lattice units as a function of n_c or $3\times\tau$ (left), $4.25\times\tau$ (center) and $7.965\times\tau$ (right) for Wilson, Symanzik tree-level improved and Iwasaki gauge actions, respectively. The results are obtained using a fit to the dipole form of Eq. (65) with a cutoff $Q^2 < (1\text{ GeV})^2$. Data obtained by cooling (gradient-flow) are shown by red squares (blue circles). Gradient-flow results have been shifted horizontally to improve visibility.

In Fig. 8 we present $F_3(0)/(2am_N)$ as a function of the number of cooling steps n_c and the corresponding gradient flow time. These results clearly confirm that the value of the nEDM obtained via cooling agrees with the one extracted via the gradient flow corroborating the equivalence of cooling and gradient flow also on the level of the nEDM. In addition, we observe that $|\vec{d}_N|/\bar{\theta}$ (Eq. (9)) is adequately stable for $n_c \geq 20$ and the corresponding gradient flow time. By looking at the nEDM as a function of τ and n_c for the gradient flow and cooling respectively we observe that fixing $\sqrt{8t} \approx 0.6$fm is in the plateau region and suggests that the value of $F_3(0)/(2m_N)$ can be taken for $n_c = 20,\ 30$ and 50 cooling steps or at the corresponding gradient flow times for Wilson, Symanzik tree-level improved and Iwasaki actions, respectively. The results for $F_3(0)/(2m_N)$ extracted using the dipole fit and the above cooling steps or the corresponding gradient flow times are collected in Table 3. As can be seen, the values obtained for $t_{\text{sep}} = 14a$ are consistent with those obtained using $t_{\text{sep}} = 12a$ albeit with larger errors. We use data obtained for $t_{\text{sep}} = 12a$ to determine our final result due to their better statistical accuracy compared to the results obtained for $t_{\text{sep}} = 14a$. In addition we stress that we do not attempt to make an extrapolation to infinite volume i.e $t_{\text{sep}} \to \infty$ and determine the corresponding systematic error.

$F_3(0)/(2m_N)$ (e.fm)				
Gauge action	cooling		gradient flow	
	$t_{\text{sep}} = 12a$	$t_{\text{sep}} = 14a$	$t_{\text{sep}} = 12a$	$t_{\text{sep}} = 14a$
Wilson	-0.035(09)	-0.056(45)	-0.039(10)	-0.065(42)
Symanzik	-0.036(10)	-0.072(50)	-0.046(12)	-0.076(40)
Iwasaki	-0.035(10)	-0.049(22)	-0.041(12)	-0.053(23)

Table 3: $F_3(0)/(2m_N)$ extracted from fitting to the dipole Ansatz of Eq. (65). We include results for both $t_{\text{sep}} = 12a$ and $t_{\text{sep}} = 14a$ at $n_c = 20$, $n_c = 30$ and $n_c = 50$ as well as at the corresponding gradient flow times given in Table 2 for the Wilson, Symanzik tree-level improved and Iwasaki actions, respectively.

8.2.2 $F_3(0)$ via the application of the derivative to the ratio technique

In this section we discuss the results on $F_3(0)$ using the application of the derivative to the ratio method. As explained in Section 6.2.1, this requires the construction of the derivative-like three point functions expressed as $\sum_{x_j=-L/2+a}^{L/2-a}(\sum_{x_i=0,i\neq j}^{L-a} ix_j G^{\mu}_{\rm 3pt,\mathcal{Q}}(\vec{x},t_f,t_i,t,\Gamma_k))$, $\sum_{x_j=-L/2+a}^{L/2-a}(\sum_{x_i=0,i\neq j}^{L-a} ix_j G^{k}_{\rm 3pt}(\vec{x},t_f,t_i,t,\Gamma_0))$ and $\sum_{x_j=-L/2+a}^{L/2-a}(\sum_{x_i=0,i\neq j}^{L-a} ix_j G^{k}_{\rm 3pt}(\vec{x},t_f,t_i,t,\Gamma_i))$ as well as the two-point function $G_{\rm 2pt}(\vec{q},t_f,0,\Gamma_0)$ in order to form the right ratios. The three derivative-like three point functions are computed by taking the Fourier transformation according to Eq. (69). As previously mentioned, we use a source-sink separation of $t_{\rm sep}=12a$ and shift the source timeslice to $t_i=0$. Once more we check for ground state dominance by extracting the nEDM for $t_{\rm sep}=10a$ and $t_{\rm sep}=14a$. In addition, we average over the spatial direction $j=1,2,3$ as this appears in Eq. (66). We fit the ratio to a constant in the plateau region to extract the quantity given in Eq. (66) and use the procedure explained in Section 8.2.1 by employing the mean value for α^1 as well as $\alpha^1_{\rm max}=\alpha^1+d\alpha^1$ in order to compute the associated statistical error on F_3. As discussed in Section 6.2.1 there can be a residual time dependence in Eq. (66) of the form $\sim \exp\left(a(E_N(\vec{q})-m_N)\ t/a\right)$. Hence, in addition to the constant fit we also perform an exponential fit in order to provide a systematic error. We take the difference between the value determined from the constant fit and that extracted when we include the exponential time-dependence as the systematic error. We note that the resulting systematic error is comparable to our statistical error making this approach useful.

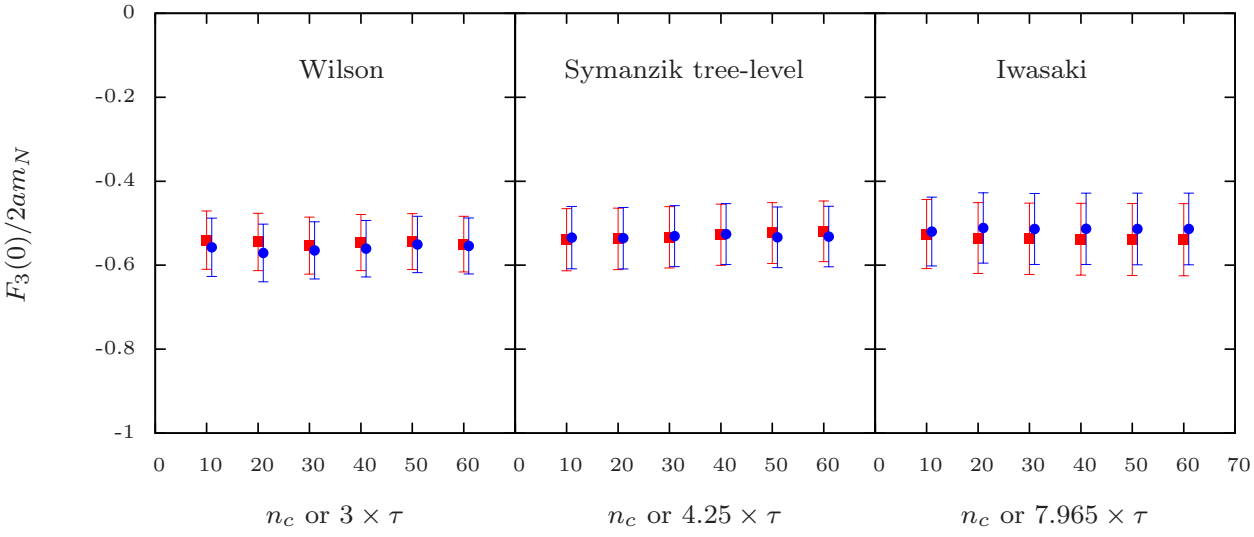

Figure 9: Results for the nEDM in lattice units using the application of the derivative to the ratio as a function of n_c or $3\times\tau$ (left), $4.25\times\tau$ (center) and $7.965\times\tau$ (right). The notation is the same as in Fig. 8.

In Fig. 9 we show the results for $F_3(0)/(2am_N)$ in lattice units. The derivative-like three-point function $\sum_{x_j=-L/2+a}^{L/2-a}(\sum_{x_i=0,i\neq j}^{L-a} ix_j G^{\mu}_{\rm 3pt,\mathcal{Q}}(\vec{x},t_f,t_i,t,\Gamma_k))$ uses the topological charge extracted from cooling and the gradient flow for the Wilson, Symanzik tree-level improved and Iwasaki smoothing actions as a function of the cooling steps or the flow time τ. Similarly to Fig. 8, the value of the nEDM is stable for the smoothing scales used to define the topological charge. Namely, this justifies our choice of fixing $\sqrt{8t}\approx 0.6$fm, thus results in using $n_c=20$, 30 and 50 as well as to the corresponding gradient flow times for Wilson, Symanzik tree-level improved and Iwasaki smoothing actions respectively.

In Fig. 10 we show results for the combination of continuum-like derivatives of ratios leading to the extraction of $F_3(0)$ according to Eq. (66). The results are produced with topological charge extracted using the gradient flow for a total of $\tau=6.3$ with the Iwasaki action. A plateau can be identified and fitted in the range $t/a\in[4,8]$ yielding a value of $F_3(0)=-0.52(09)$. The statistical error is computed using the method

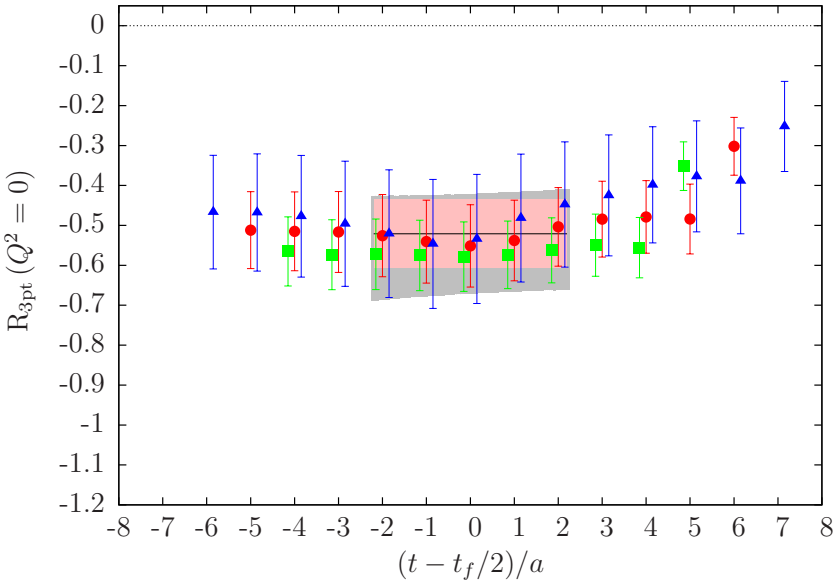

Figure 10: The ratio leading to $F_3(0)$ determined using the continuum derivative method. Green squares, red circles and blue triangles correspond to source-sink separation of $t_f/a = 10, 12, 14$, respectively. The topological charge is evaluated using the gradient flow at $\tau = 6.3$ with the Iwasaki action. The behaviour when using other smoothing actions to calculate the topological charge is similar.

explained in the previous subsection and is presented by the red band. In addition we provide the exponential fit with its statistical uncertainty resulting from the residual exponential time-dependence in the three-point function. The fit is done in the range $t/a \in [4, 8]$ yielding a value of $F_3(0) = -0.55(13)$. As can be seen, the two bands yield consistent results.

In Table 4 we give the results for $F_3(0)/(2m_N)$ for the three gauge smoothing actions using our standard parameters for n_c and τ. We provide the statistical as well as the systematic error induced by the residual exponential time-dependence in the three-point function (see Eq. (69)).

$F_3(0)/(2m_N)$ (e.fm)				
Gauge action	cooling		gradient flow	
	$t_{\rm sep} = 12a$	$t_{\rm sep} = 14a$	$t_{\rm sep} = 12a$	$t_{\rm sep} = 14a$
Wilson	-0.044(6)(6)	-0.044(8)(8)	-0.046(6)(9)	-0.046(8)(15)
Symanzik	-0.043(6)(3)	-0.043(9)(6)	-0.043(6)(4)	-0.042(9)(10)
Iwasaki	-0.044(7)(4)	-0.043(11)(10)	-0.042(7)(3)	-0.040(11)(8)

Table 4: Results for $F_3(0)/(2m_N)$ extracted using the application of the derivative to the ratio method for $t_{\rm sep} = 12a, 14a$. Results are shown for $n_c = 20,\ 30,$ and 50 as well as for the corresponding gradient flow times according to Table 2 for Wilson, Symanzik tree-level improved and Iwasaki actions respectively. The error in the first parenthesis is statistical and in the second the systematic determined as discussed in the text.

8.2.3 $F_3(0)$ with the elimination of the momentum in the plateau region technique

The elimination of the momentum in the plateau region method is an improved technique to remove momentum prefactors in the form factor decomposition of a given ratio of correlators on the lattice. The details of this method can be found in Section 6.2.2 and Ref. [29] where the method was applied for the first time for the

evaluation of the nucleon anomalous magnetic moment. Similar approaches using analytic continuation have been used in the context of calculating hadronic vacuum polarizations [65, 66]. In the following we present the first results for the nEDM obtained within this approach.

As in the other methods, here we also extract $F_3(0)$ using the various definitions for the topological charge (Wilson, Symanzik tree-level improved and Iwasaki actions for both cooling and gradient flow). The results obtained within this approach exhibit a similar behavior as that depicted in Fig. 8 and Fig. 9. We analyze data for two source-sink separations, namely of $t_{\text{sep}} = 12a$ and $t_{\text{sep}} = 14a$, employing a general momentum cutoff $Q_1 < 4 \cdot (2\pi/L)$ and momentum classes with an off-axis momentum squared of up to $Q^2_{\text{off}} \leq 5 \cdot (2\pi/L)^2$ (c.f. Eq. (74)). The red bands in both panels of Fig. 11 show the results for $F_3(Q^2)/(2m_N)$ extracted using the momentum elimination method and $t_{\text{sep}} = 12a$. It is obtained as the error weighted average over all sets of different off-axis momentum classes $M(Q_1, Q^2_{\text{off}})$. As required, the band reproduces the red points which are the results obtained using plateau method at each Q^2 value.

The right panel of Fig. 11 contains separate bands for the results from different value of Q^2_{off}, which agree within their errors. However, the errors at small values of Q^2 grow rapidly with increasing Q^2_{off}, such that higher off-axis momentum classes with $Q^2_{\text{off}} \geq 2 \cdot (2\pi/L)^2$ hardly contribute to the nEDM at all.

The results obtained using this approach are collected in Table 5. Although using the Wilson smoothing action to calculate the topological charge (either through cooling or the gradient flow) we obtained lower mean values and equivalently higher when using the Iwasaki action, the results are compatible within errors. Comparing the results for $t_{\text{sep}} = 12a$ and $t_{\text{sep}} = 14a$ we can not detect excited state contamination within statistical errors.

In addition, results obtained using the elimination of the momentum in the plateau region technique, which does not assume any functional form for the momentum dependence are compatible with the dipole fit results. The dipole form fit yields correlated $\chi^2/\text{DOF} = 0.54$, supporting a dipole behaviour, which is the approach used in other lattice studies.

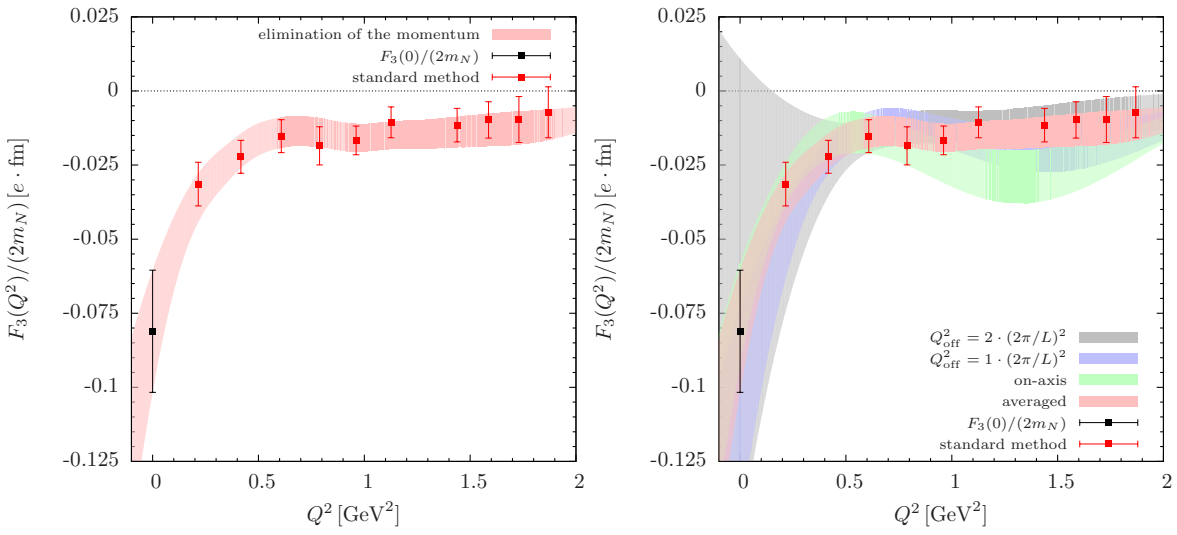

Figure 11: Results on nEDM using the momentum elimination method for source-sink separation $t_{\text{sep}} = 12a$. The right panel shows separate bands for the three sets of lowest off-axis momentum classes $M(Q_1, Q^2_{\text{off}})$.

$F_3(0)/(2m_N)$ (e.fm)				
Gauge action	cooling		gradient flow	
	$t_{\rm sep} = 12a$	$t_{\rm sep} = 14a$	$t_{\rm sep} = 12a$	$t_{\rm sep} = 14a$
Wilson	-0.052(17)	-0.043(26)	-0.056(17)	-0.043(26)
Symanzik	-0.066(18)	-0.053(28)	-0.068(17)	-0.055(28)
Iwasaki	-0.082(21)	-0.076(32)	-0.082(21)	-0.073(32)

Table 5: Results for the neutron electric dipole moment in physical units for two values of the source-sink separation and the three different smoothing actions. Results are given for n_c and τ which correspond to $\sqrt{8t} \approx 0.6$fm according to Table 2.

9 Conclusions

The neutron electric dipole moment is computed using N_f=2+1+1 twisted mass fermions simulated at a pion mass of 373 MeV and lattice spacing of $a = 0.082$ fm employing a total of 4623 measurements. This high statistics analysis enables us to extract reliable results on the CP-violating form factor $F_3(0)$ and benchmark our techniques. Due to the multiplicative kinematical factors appearing in front of $F_3(Q^2)$ it cannot be extracted directly from the matrix element. The usual approach is to extrapolate $F(Q^2)$ to $Q^2 = 0$ by fitting its Q^2-dependence employing an Ansatz for its momentum dependence. In this work, besides this standard approach, we employ two new techniques that explicitly eliminate the kinematical factor yielding directly $F_3(0)$ without any model assumption on its Q^2-dependence. These techniques involve the three-point function in coordinate space and two different ways to eliminate the kinematical factor. The behaviour of the nEDM extracted by these two techniques, as well as through fitting to a dipole Ansatz is demonstrated in Fig. 12. We show results for the nEDM with the topological charge computed using either cooling or the gradient flow and the Iwasaki gauge action. As can be seen, results extracted from fitting to a dipole Ansatz have very similar mean value to those extracted using continuum derivative with the latter having smaller errors. The results extracted from the elimination of the momentum in the plateau region tend to be lower with larger errors. This behavior resembles the results obtained for the isovector magnetic form factor of the nucleon at zero momentum [29] where it was found that the results obtained using the elimination of the momentum in the plateau region method tend to be larger (and closer to the experimental value) than those obtained using a dipole fit .

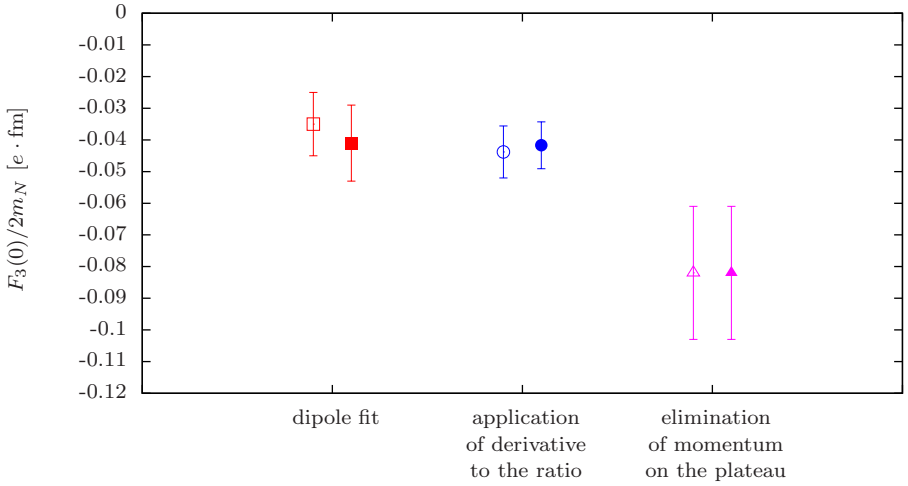

Figure 12: Our results for $F_3(0)/(2m_N)$ in physical units using different approaches to determine $F_3(0)$. Open (filled) symbols show results using cooling (gradient flow) for the extraction of the topological charge. Red/blue/magenta points show results extracted using a dipole fit/application of the derivative to the ratio/elimination of the momentum in the plateau region approach, respectively. The topological charge has been evaluated using the Iwasaki smoothing action.

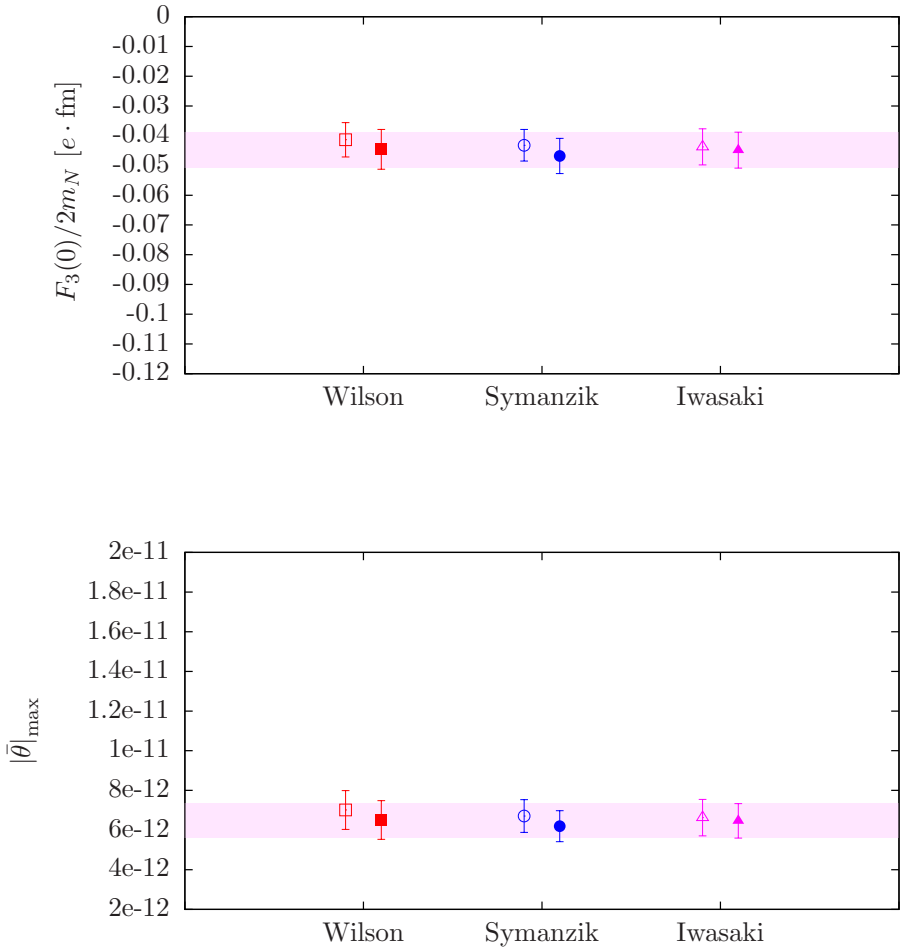

Figure 13: Upper panel: Our results for $F_3(0)/(2m_N)$ in physical units using different methods. Open (filled) symbols show results using cooling (gradient flow) for the evaluation of the topological charge. Red/blue/magenta points represent the smoothing actions Wilson/Symanzik tree-level improved/Iwasaki). The presented results have been obtained from the weighted averages of values for $F_3(0)/(2m_N)$ extracted using: the dipole fit on $F_3(Q^2)$, the application of the derivative to the ratio technique, and the elimination of the momentum in the plateau region technique. As a final result we report the value of nEDM extracted when using $\mathcal{Q}$ from the gradient flow with Iwasaki action, shown with the magenta error band. Lower panel: The corresponding upper bounds in $|\bar{\theta}|$ extracted using the experimental result $|\vec{d}_N| = 2.9 \times 10^{-13} e \cdot$ fm [3, 4, 5].

An additional new element of this work, is the computation of the topological charge using both cooling and the gradient flow method. We show that the two approaches are equivalent if the flow time and number of cooling steps are tuned appropriately. This agreement is demonstrated in Fig. 12 and Fig. 13 where we show results for the nEDM with the topological charge computed using cooling or the gradient flow method. Furthermore, results using different actions to smooth the gauge links entering the computation of the topological charge yield overall consistent results. The values appearing in Fig. 13 have been obtained by taking the weighted average among the data extracted using the dipole fit, the application of the derivative to the ratio technique and the elimination of the momentum in the plateau region, shown in Fig. 12. Given that the simulations used the Iwasaki action, we present as our final value for the nEDM the value extracted when the Iwasaki action is employed to define the topological charge. As systematic error we take the difference between the mean values obtained when cooling and the gradient flow are used to determine the topological charge. Our final result is thus $F_3(0)/(2m_N) = -0.045(6)(1)\, e\cdot$fm at a pion mass of $m_\pi = 373$ MeV. As already remarked in the introduction, this value is in agreement with the value extracted using N_f=2+1 domain wall fermions at pion mass of about 300 MeV [32]. Using this value of $F_3(0)/(2m_N)$ and the experimental result $|\vec{d}_N| = 2.9 \times 10^{-13} e \cdot$ fm as an upper bound we can extract the maximum allowed value of $\bar{\theta}$ displayed in Fig. 13. We find a maximum value of $\bar{\theta} = 6.4(0.9)(0.2) \times 10^{-12}$.

Having investigated the nEDM using an ensemble simulated at $m_\pi = 373$ MeV we are in the process of analyzing an ensemble with two degenerate light quarks with mass fixed to the physical value, thus eliminating any systematic error that may arise due to a heavier than physical pion mass.

Acknowledgments

We would like to thank all members of ETMC for the most enjoyable collaboration. Numerical calculations have used HPC resources from John von Neumann-Institute for Computing on the JUQUEEN and JUROPA systems at the research center in Jülich. This work was supported, in part, by a grant from the Swiss National Supercomputing Centre (CSCS) under project ID s540. Additional computational resources were provided by the Cy-Tera machine at The Cyprus Institute funded by the Cyprus Research Promotion Foundation (RPF), ΝΕΑΥΠΟΔΟΜΗ/ΣΤΡΑΤΗ/0308/31. In addition, we would like to thank H. Panagopoulos, M. Teper, B. Lucini, A. Ramos and C. Michael for useful discussion on various aspects of this project. K.O. is supported by the Bonn-Cologne Graduate School (BCGS) of Physics and Astronomie. M.C. is supported by the Cyprus RPF under the contract TECHNOLOGY/ΘΕΠΙΣ/0311(BE)/16. K.H. acknowledges support by the Cyprus RPF under contract ΤΠΕ/ΠΛΗΡΟ/0311(BIE)/09.

References

[1] S. Dar, *"The Neutron EDM in the SM: A Review"*, hep-ph/0008248.

[2] M. Pospelov and A. Ritz, *"Electric dipole moments as probes of new physics"*, Annals Phys. **318**, 119 (2005), [hep-ph/0504231].

[3] V. Helaine [nEDM Collaboration], *"The neutron Electric Dipole Moment experiment at the Paul Scherrer Institute"*, EPJ Web Conf. **73** (2014) 07003.

[4] C. A. Baker *et al.*, *"An Improved experimental limit on the electric dipole moment of the neutron"*, Phys. Rev. Lett. **97**, 131801 (2006), [hep-ex/0602020].

[5] C. A. Baker *et al.*, *"Reply to comment on 'An Improved experimental limit on the electric dipole moment of the neutron' "*, Phys. Rev. Lett. **98**, 149102 (2007), [arXiv:0704.1354].

[6] V. Baluni, *"CP Violating Effects in QCD"*, Phys. Rev. D **19**, 2227 (1979).

[7] R. J. Crewther, P. Di Vecchia, G. Veneziano and E. Witten, *"Chiral Estimate of the Electric Dipole Moment of the Neutron in Quantum Chromodynamics"*, Phys. Lett. B **88**, 123 (1979), [Phys. Lett. B **91**, 487 (1980)].

[8] M. A. Shifman, A. I. Vainshtein and V. I. Zakharov, *"Can Confinement Ensure Natural CP Invariance of Strong Interactions?"*, Nucl. Phys. B **166** (1980) 493.

[9] H. J. Schnitzer, *"The Soft Pion Skyrmion Lagrangian and Strong CP Violation"*, Phys. Lett. B **139**, 217 (1984).

[10] E. P. Shabalin, *"The Electric Dipole Moment Of The Neutron In A Gauge Theory"*, Sov. Phys. Usp. **26**, 297 (1983) [Usp. Fiz. Nauk **139**, 561 (1983)].

[11] M. M. Musakhanov and Z. Z. Israilov, *"The Electric Dipole Moment Of The Neutron In The Chiral Bag Model"*, Phys. Lett. B **137**, 419 (1984).

[12] P. Cea and G. Nardulli, *"A Realistic Calculation of the Electric Dipole Moment of the Neutron Induced by Strong CP Violation"*, Phys. Lett. B **144**, 115 (1984).

[13] M. A. Morgan and G. A. Miller, *"The Neutron Electric Dipole Moment in the Cloudy Bag Model"*, Phys. Lett. B **179** (1986) 379.

[14] J. A. McGovern and M. C. Birse, *"The neutron electric dipole moment in chiral quark-meson models"*, Phys. Rev. **D45**, 2437 (1992).

[15] P. Di Vecchia, *"The Dynamics of the Pseudoscalar Mesons at Arbitrary Θ in Large N Quantum Chromodynamics"*, Acta Phys. Austriaca Suppl. **22**, 341 (1980).

[16] A. Pich and E. de Rafael, *"Strong CP violation in an effective chiral Lagrangian approach"*, Nucl. Phys. B **367** 313 (1991).

[17] B. Borasoy, *"The Electric dipole moment of the neutron in chiral perturbation theory"*, Phys. Rev. D **61**, 114017 (2000), [arXiv:hep-ph/0004011].

[18] W. H. Hockings and U. van Kolck, *"The Electric dipole form factor of the nucleon"*, Phys. Lett. B **605**, 273 (2005), [arXiv:nucl-th/0508012].

[19] S. Narison, *"A Fresh Look into the Neutron EDM and Magnetic Susceptibility"*, Phys. Lett. B **666**, 455 (2008), [arXiv:0806.2618].

[20] K. Ottnad, B. Kubis, U.-G. Meissner and F.-K. Guo, *"New insights into the neutron electric dipole moment"*, Phys. Lett. B **687** 42 (2010), [arXiv:0911.3981].

[21] J. de Vries, R. G. E. Timmermans, E. Mereghetti and U. van Kolck, *"The Nucleon Electric Dipole Form Factor From Dimension-Six Time-Reversal Violation"*, Phys. Lett. B **695**, 268 (2011), [arXiv:1006.2304].

[22] E. Mereghetti, J. de Vries, W. H. Hockings, C. M. Maekawa and U. van Kolck, *"The Electric Dipole Form Factor of the Nucleon in Chiral Perturbation Theory to Sub-leading Order"*, Phys. Lett. B **696**, 97 (2011), [arXiv:1010.4078].

[23] J. de Vries, E. Mereghetti, R. G. E. Timmermans and U. van Kolck, *"The Effective Chiral Lagrangian From Dimension-Six Parity and Time-Reversal Violation"*, Annals Phys. **338**, 50 (2013), [arXiv:1212.0990].

[24] F. K. Guo and U. G. Meissner, *"Baryon electric dipole moments from strong CP violation"*, JHEP **1212**, 097 (2012), [arXiv:1210.5887].

[25] T. Akan, F. K. Guo and U. G. Meissner, *"Finite-volume corrections to the CP-odd nucleon matrix elements of the electromagnetic current from the QCD vacuum angle"*, Phys. Lett. B **736**, 163 (2014), [arXiv:1406.2882].

[26] R. D. Peccei and H. R. Quinn, *"CP Conservation in the Presence of Instantons"*, Phys. Rev. Lett. **38**, 1440 (1977).

[27] R. D. Peccei, *"The Strong CP Problem"*, Adv. Ser. Direct. High Energy Phys. **3**, 503 (1989).

[28] S. M. Barr and W. J. Marciano in *"CP Violation"*, ed. C Jarlskog (World Scientific, Singapore, 1988).

[29] C. Alexandrou *et al.*, *"Extraction of the isovector magnetic form factor of the nucleon at zero momentum"*, PoS LATTICE2014 (2014) 075, [arXiv:1410.8818].

[30] M. Lüscher, *"Properties and uses of the Wilson flow in lattice QCD"*, JHEP **1008**, 071 (2010) [JHEP **1403**, 092 (2014)], [arXiv:1006.4518].

[31] C. Alexandrou, A. Athenodorou and K. Jansen, *"Topological charge using cooling and the gradient flow"*, Phys. Rev. D **92** (2015) 12, 125014, [arXiv:1509.04259].

[32] E. Shintani, T. Blum, A. Soni and T. Izubuchi, *"Neutron and proton EDM with $N_f = 2 + 1$ domain-wall fermion"*, PoS LATTICE **2013**, 298 (2014).

[33] E. Shintani, S. Aoki and Y. Kuramashi, *"Full QCD calculation of neutron electric dipole moment with the external electric field method"*, Phys. Rev. D **78**, 014503 (2008), [arXiv:0803.0797].

[34] F.-K. Guo *et al.*, *"The electric dipole moment of the neutron from 2+1 flavor lattice QCD"*, Phys. Rev. Lett. **115**, no. 6, 062001 (2015), [arXiv:1502.02295].

[35] A. Shindler, T. Luu and J. de Vries, *"The nucleon electric dipole moment with the gradient flow: the θ-term contribution"*, [arXiv:1507.02343].

[36] Y. Iwasaki, K. Kanaya, T. Kaneko and T. Yoshie, *"Scaling in SU(3) pure gauge theory with a renormalization group improved action,"*x Phys. Rev. D **56** (1997) 151 [hep-lat/9610023].

[37] R. Frezzotti *et al.* [Alpha Collaboration], *"Lattice QCD with a chirally twisted mass term,"* JHEP **0108** (2001) 058 [hep-lat/0101001].

[38] R. Frezzotti and G. C. Rossi, *"Chirally improving Wilson fermions - I. O(a) improvement"*, JHEP **0408** (2004) 007, [arXiv:hep-lat/0306014].

[39] R. Frezzotti, G. Martinelli, M. Papinutto and G. C. Rossi, *"Reducing cutoff effects in maximally twisted lattice QCD close to the chiral limit,"* JHEP **0604**, 038 (2006) [hep-lat/0503034].

[40] R. Frezzotti and G. C. Rossi, *"Twisted mass lattice QCD with mass nondegenerate quarks"*, Nucl. Phys. Proc. Suppl. **128** (2004) 193 [hep-lat/0311008].

[41] R. Baron *et al.*, *"Light hadrons from lattice QCD with light (u,d), strange and charm dynamical quarks"*, JHEP **1006**, 111 (2010), [arXiv:1004.5284].

[42] A. Athenodorou and R. Sommer, *"One-loop lattice artifacts of a dynamical charm quark"* Phys. Lett. B **705**, 393 (2011), [arXiv:1109.2303].

[43] M. Bruno *et al.* [ALPHA Collaboration], *"Effects of Heavy Sea Quarks at Low Energies"* Phys. Rev. Lett. **114**, no. 10, 102001 (2015), [arXiv:1410.8374].

[44] C. Alexandrou *et al.*, *"Hyperon and charmed baryon masses and nucleon excited states from lattice QCD"*, arXiv:1410.4553.

[45] R. Baron *et al.* [ETM Collaboration], *"Light hadrons from N_f=2+1+1 dynamical twisted mass fermions"*, PoS LATTICE **2010**, 123 (2010), [arXiv:1101.0518].

[46] S. Aoki and A. Gocksch, *"The Neutron Electric Dipole Moment in Lattice QCD"*, Phys. Rev. Lett. **63**, 1125 (1989) [Phys. Rev. Lett. **65**, 1172 (1990)].

[47] D. Guadagnoli, V. Lubicz, G. Martinelli and S. Simula, *"Neutron electric dipole moment on the lattice: A Theoretical reappraisal"* JHEP **0304**, 019 (2003), [hep-lat/0210044].

[48] P. Faccioli, D. Guadagnoli and S. Simula, *"The Neutron electric dipole moment in the instanton vacuum: Quenched versus unquenched simulations"*, Phys. Rev. D **70**, 074017 (2004), [hep-ph/0406336].

[49] E. Shintani *et al.*, *"Neutron electric dipole moment from lattice QCD"*, Phys. Rev. D **72**, 014504 (2005), [hep-lat/0505022].

[50] E. Shintani *et al.*, *"Neutron electric dipole moment with external electric field method in lattice QCD"* Phys. Rev. D **75**, 034507 (2007), [hep-lat/0611032].

[51] B. Alles, M. D'Elia and A. Di Giacomo, *"An Upper limit to the electric dipole moment of the neutron from lattice QCD"*, Nucl. Phys. Proc. Suppl. **164**, 256 (2007), [hep-lat/0510067].

[52] S. Aoki, R. Horsley, T. Izubuchi, Y. Nakamura, D. Pleiter, P. E. L. Rakow, G. Schierholz and J. Zanotti, *"The Electric dipole moment of the nucleon from simulations at imaginary vacuum angle theta"* arXiv:0808.1428].

[53] A. Stathopoulos and K. Orginos, *"Computing and deflating eigenvalues while solving multiple right hand side linear systems in quantum chromodynamics"*, SIAM J. Sci. Comput. **32**, 439 (2010), [arXiv:0707.0131].

[54] A. Stathopoulos, A. M. Abdel-Rehim and K. Orginos, *"Deflation for inversion with multiple right-hand sides in QCD"*, J. Phys. Conf. Ser. **180**, 012073 (2009).

[55] A. Abdel-Rehim *et al.*, *"Disconnected quark loop contributions to nucleon observables in lattice QCD"*, Phys.Rev. **D89** (2014) 034501, [arXiv:1310.6339].

[56] C. Alexandrou *et al.*, *"The Static Approximation of Heavy-Light Quark-Systems - A Systematic Lattice Study"*, Nucl. Phys. **B414** (1994) 815-855, [arXiv:hep-lat/9211042].

[57] S. Gusken, *"A Study of smearing techniques for hadron correlation functions"* Nucl. Phys. Proc. Suppl. **17**, 361 (1990).

[58] C. Alexandrou *et al.*, *"Light baryon masses with dynamical twisted mass fermions"*, Phys. Rev. **D78** (2008) 014509, [arXiv:0803.3190].

[59] M. Constantinou, V. Lubicz, H. Panagopoulos and F. Stylianou, *"$\mathcal{O}(a^2)$ corrections to the one-loop propagator and bilinears of clover fermions with Symanzik improved gluons"*, JHEP **0910**, 064 (2009), [arXiv:0907.0381].

[60] C. Alexandrou, M. Constantinou, S. Dinter, V. Drach, K. Jansen, C. Kallidonis and G. Koutsou, *"Nucleon form factors and moments of generalized parton distributions using $N_f = 2+1+1$ twisted mass fermions"*, Phys. Rev. D **88**, no. 1, 014509 (2013), [arXiv:1303.5979].

[61] C. Alexandrou *et al.*, *"Direct computation of the nucleon magnetic moment"*, in preparation.

[62] M. Luscher, *"Trivializing maps, the Wilson flow and the HMC algorithm"*, Commun. Math. Phys. **293**, 899 (2010), [arXiv:0907.5491].

[63] C. Bonati and M. D'Elia, *"Comparison of the gradient flow with cooling in $SU(3)$ pure gauge theory"*, Phys. Rev. D **89**, no. 10, 105005 (2014), [arXiv:1401.2441].

[64] T.W. Anderson and D.A. Darling, *"A Test of Goodness-of-Fit"*, Journal of the American Statistical Association **49** 765769 (1954).

[65] D. Bernecker and H. B. Meyer, *"Vector Correlators in Lattice QCD: Methods and applications"*, Eur. Phys. J. A **47**, 148 (2011), [arXiv:1107.4388].

[66] X. Feng et al., *"Computing the hadronic vacuum polarization function by analytic continuation"*, Phys. Rev. D **88**, 034505 (2013), [arXiv:1305.5878].